Geochemistry Geophysics Geosystems G3

Article
Volume 11
23 November 2010
Q0AC08, doi:10.1029/2010GC003233
ISSN: 1525-2027

Published by AGU and the Geochemical Society

Low-productivity Hawaiian volcanism between Kaua'i and O'ahu

Andrew R. Greene and Michael O. Garcia
Department of Geology and Geophysics, University of Hawai'i at Mānoa, 1680 East-West Road, Honolulu, Hawaii 96822, USA (agreene@soest.hawaii.edu)

Dominique Weis
Pacific Centre for Isotopic and Geochemical Research, Department of Earth and Ocean Sciences, University of British Columbia, 6339 Stores Road, Vancouver, British Columbia V6T 1Z4, Canada

Garrett Ito
Department of Geology and Geophysics, University of Hawai'i at Mānoa, 1680 East-West Road, Honolulu, Hawaii 96822, USA

Maia Kuga
Laboratoire des Sciences de la Terre, Ecole Normale Supérieure de Lyon, 46 Allée d'Italie, F-69364 Lyon CEDEX 07, France

Joel Robinson
Volcano Science Center, U.S. Geological Survey, 345 Middlefield Road, MS 910, Menlo Park, California 94025, USA

Seiko Yamasaki
Division of Earth and Planetary Sciences, Graduate School of Science, Kyoto University, Kitashirakawa Oiwake-cho, Sakyo-ku, Kyoto 606-8502, Japan

[1] The longest distance between subaerial shield volcanoes in the Hawaiian Islands is between the islands of Kaua'i and O'ahu, where a field of submarine volcanic cones formed astride the axis of the Hawaiian chain during a period of low magma productivity. The submarine volcanoes lie ~25–30 km west of Ka'ena Ridge that extends ~80 km from western O'ahu. These volcanoes were sampled by three Jason2 dives. The cones are flat topped, <400 m high and 0.4–2 km in diameter at water depths between ~2700 and 4300 m, and consist predominantly of pillowed flows. Ar-Ar and K-Ar ages of 11 tholeiitic lavas are between 4.9 and 3.6 Ma. These ages overlap with shield volcanism on Kaua'i (5.1–4.0 Ma) and Wai'anae shield basalts (3.9–3.1 Ma) on O'ahu. Young alkalic lavas (circa 0.37 Ma) sampled southwest of Ka'ena Ridge are a form of offshore secondary volcanism. Half of the volcanic cones contain high-SiO_2 basalts (51.0–53.5 wt % SiO_2). The trends of isotopic compositions of West Ka'ena tholeiitic lavas diverge from the main Ko'olau-Kea shield binary mixing trend in isotope diagrams and extend to lower $^{208}Pb/^{204}Pb$ and $^{206}Pb/^{204}Pb$ than any Hawaiian tholeiitic lava. West Ka'ena tholeiitic lavas have geochemical and isotopic characteristics similar to volcanoes of the Loa trend. Hence, our results show that the Loa-type volcanism has persisted for at least 4.9 Myr, beginning prior to the development of the dual, subparallel chain of volcanoes. Several West Ka'ena samples are similar to higher SiO_2, Loa trend lavas of Ko'olau Makapu'u stage, Lāna'i, and Kaho'olawe; these lavas may have been derived from a pyroxenite source in the mantle. The high Ni contents of olivines in West Ka'ena lavas also indicate contribution from pyroxenite-derived melting. Average compositions of Hawaiian shield volcanoes show a clear relation between $^{206}Pb/^{204}Pb$ and SiO_2 within Loa trend volcanoes, which supports a prominent but variable influence of pyroxenite in

the Hawaiian plume source. In addition, both Pb isotopes and volcano volume show a steady increase with time starting from a minimum west of Ka'ena Ridge. The entrained mafic component in the Hawaiian plume is probably not controlling the increasing magma productivity in the Hawaiian Islands.

Components: 18,500 words, 13 figures, 3 tables.

Keywords: West Ka'ena; tholeiitic volcanism; submarine volcanism; Loa-Kea trends; pyroxenite.

Index Terms: 1037 Geochemistry: Magma genesis and partial melting (3619); 3619 Mineralogy and Petrology: Magma genesis and partial melting (1037); 1038 Geochemistry: Mantle processes (3621); 3621 Mineralogy and Petrology: Mantle processes (1038); 1025 Geochemistry: Composition of the mantle.

Received 24 May 2010; **Revised** 7 September 2010; **Accepted** 14 September 2010; **Published** 23 November 2010.

Greene, A. R., M. O. Garcia, D. Weis, G. Ito, M. Kuga, J. Robinson, and S. Yamasaki (2010), Low-productivity Hawaiian volcanism between Kaua'i and O'ahu, *Geochem. Geophys. Geosyst.*, *11*, Q0AC08, doi:10.1029/2010GC003233.

Theme: Geochemical Heterogeneities in Oceanic Island Basalt and Mid-ocean Ridge Basalt Sources: Implications for Melting Processes and Mantle Dynamics
Guest Editors: C. Beier and P. Asimow

1. Introduction

[2] The geographical and temporal distribution of isotopic and geochemical variations of lavas from Hawaiian shield volcanoes indicates that compositional heterogeneity is an intrinsic feature of the Hawaiian plume over a range of spatial scales [*Frey and Rhodes*, 1993]. The isotopic and geochemical variation of Hawaiian lavas has been used to understand the nature of the mantle source (e.g., recycled components, source lithology, scales of heterogeneities), the effect of melting processes, and causes for the evolution of the Hawaiian shield volcanoes over the last 5.5 million years. The recognition of subparallel, isotopically distinct chains of shield volcanoes (Loa and Kea trends) is up to now unique to the Hawaiian volcanic chain and presents a fundamental controversy on what in the structure of the plume stem or the plume source is controlling the emergence of these two trends [*Abouchami et al.*, 2005]. The existence of the Loa and Kea trends has been explained by several competing models involving a concentrically zoned, asymmetrically heterogeneous or vertically zoned mantle plume [*Abouchami et al.*, 2005; *Blichert-Toft et al.*, 2003; *Bryce et al.*, 2005; *Huang and Frey*, 2005; *Lassiter et al.*, 1996]. The geochemical differences between Hawaiian shields may also be controlled by the thermal structure of the plume, the Pacific Plate structure and motion, and varying source lithology and scales of heterogeneities [e.g., *Hauri*, 1996; *Blichert-Toft et al.*, 2003; *Kurz et al.*, 2004; *Abouchami et al.*, 2005; *Tanaka et al.*, 2008; *Wessel and Kroenke*, 2009].

[3] Hawaiian shield volcanoes grow in three main stages (preshield, shield (>95%–98% volume), and postshield) over a period of about 1.5 Myr [*Moore et al.*, 1982; *Garcia et al.*, 2006]. The volcanic growth rate is greatest during the shield-building stage when the volcano is centered over the melting region of the hot spot and therefore lava compositions are mostly tholeiitic basalt. In contrast, the preshield and postshield lavas form from lower degrees of partial melting and are mostly alkalic [*Moore et al.*, 1982; *Frey et al.*, 1991]. Studies of the main tholeiitic shield-building stage of Hawaiian volcanoes have examined subaerial [e.g., *Frey et al.*, 1994; *Mukhopadhyay et al.*, 2003; *Pietruszka and Garcia*, 1999] and subaqueous [e.g., *Coombs et al.*, 2004; *Hanyu et al.*, 2010; *Kimura et al.*, 2006; *Ren et al.*, 2006; *Xu et al.*, 2007] basalts that erupted on a large shield volcano and involved magma storage in reservoirs within the crust or volcanic edifice [e.g., *Tilling and Dvorak*, 1993]. Low-volume submarine tholeiitic cones west of Ka'ena Ridge between the islands of Kaua'i and O'ahu (Figure 1) are some of the only known examples of tholeiitic volcanism that occurred astride the axis of the Hawaiian Islands and was not associated with a large subaerial shield volcano. This volcanism occurred prior to the formation of the dual Loa and Kea trends.

[4] The longest distance between large subaerial shields of the Hawaiian Islands is between the

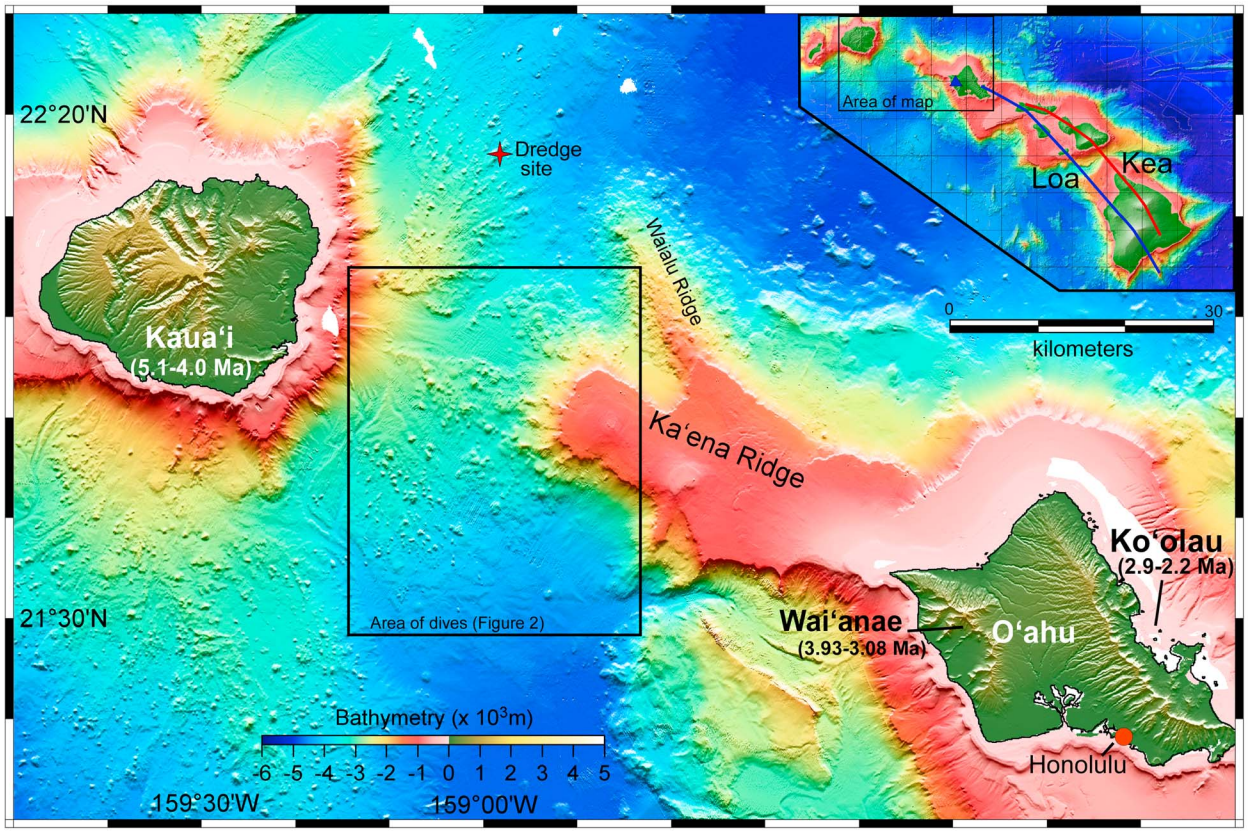

Figure 1. Hypsometry and bathymetry around the islands of Kaua'i and O'ahu with location of Jason2 dives in black box (shown in Figure 2) and a single dredge site shown with a red cross. Inset shows bathymetry of the Hawaiian Islands and Loa and Kea trend volcanoes based on distribution of Pb isotope ratios in lavas.

islands of Kaua'i and O'ahu, where the volume of lava erupted per unit area is also the smallest (i.e., low productivity compared to shield stage volcanism). Volcanism in this area formed Ka'ena Ridge, with two low shields that grew just above sea level [*Coombs et al.*, 2004]. Ka'ena Ridge is the longest submerged terrace that parallels the axis of the Hawaiian Islands (or volcano propagation vector of ~293° [*Wright and Klein*, 2006]). It is flanked by clusters of volcanic cones and a large submarine rift zone (Figure 1). This study examines the petrology, geochemistry and geochronology of volcanism between Kaua'i and O'ahu from submarine cones straddling the axis of the Hawaiian Islands that formed during a period of low magma productivity and prior to formation of dual Loa and Kea trends. The goals of this study are to evaluate (1) ages and source composition for West Ka'ena lavas compared to Hawaiian shield tholeiites, (2) pyroxenite versus peridotite source for West Ka'ena lavas, and (3) the relationship between source composition and lithology to volume flux in the Hawaiian Islands during the last 5 Ma. These new results improve our understanding of the evolution of the Hawaiian plume.

2. Geologic Background

[5] The volcanic cones and terraces west of Ka'ena Ridge are uncommon features in the Hawaiian Islands. Most flat-topped submarine cones in the Hawaiian Islands are found near submarine rift zones or proximal to subaerial shield volcanoes [*Clague et al.*, 2000]. The field of cones west of Ka'ena Ridge are ~50 km from the center of the island of Kaua'i and >100 km from Wai'anae Volcano, the second largest volcano on the island of O'ahu. The submarine volcanic cones between Kaua'i and the base of Ka'ena Ridge are most abundant within ~25–30 km of the base of Ka'ena Ridge (Figure 2).

[6] Two giant landslides have modified the original shape of Ka'ena Ridge on the north and south side

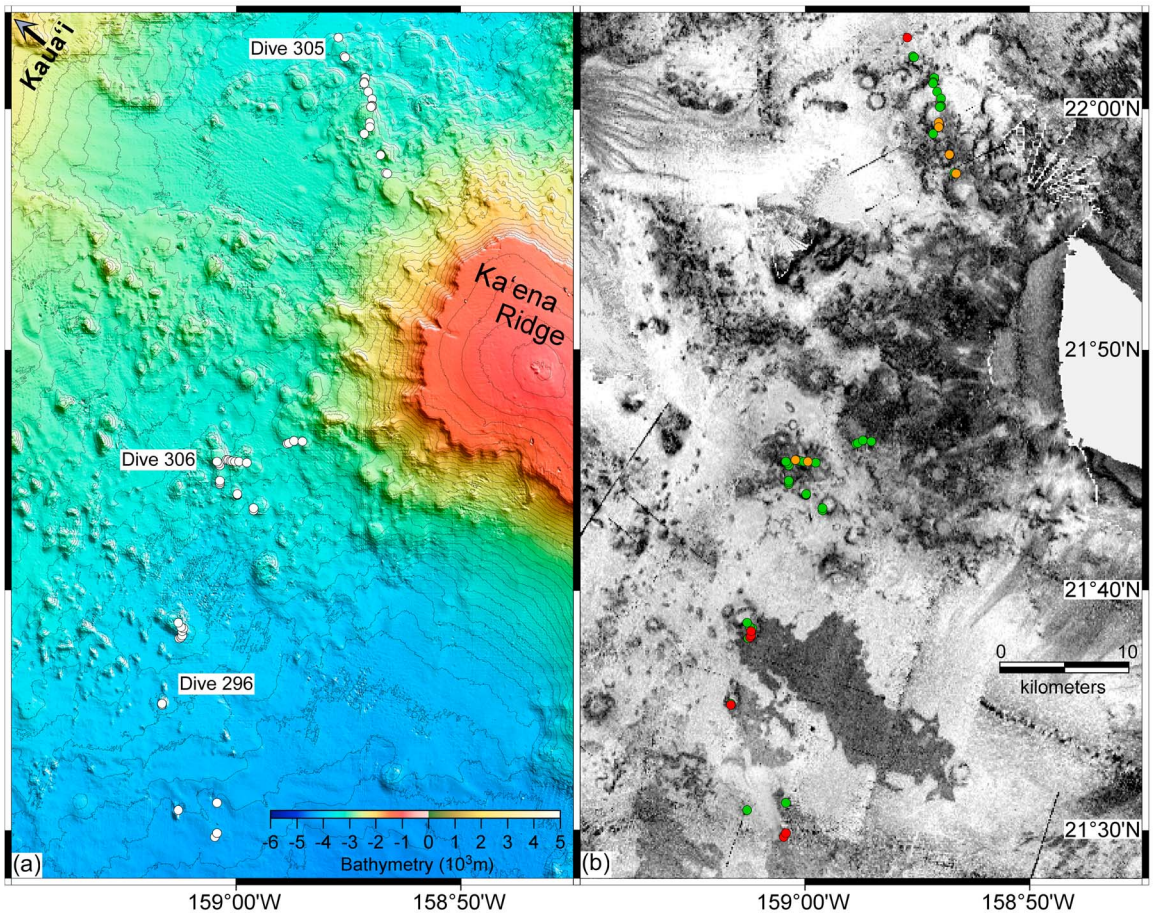

Figure 2. Bathymetric map and side-scan sonar imagery between Kaua'i and O'ahu. (a) Volcanic sample locations collected during three Jason2 dives are shown by white circles. (b) Tholeiitic (green), transitional (orange), and alkalic (red) basalts are indicated by colored dots. Area of maps is indicated by black box in Figure 1. See auxiliary material for larger, more detailed bathymetric maps of the three dive areas.

of the ridge [*Coombs et al.*, 2004]. Giant landslides have reduced Wai'anae and Ko'olau on the southwest and northeast of O'ahu, respectively [*Coombs et al.*, 2004; *Garcia et al.*, 2006; *Ozawa et al.*, 2005], and landslides may have displaced large parts of east Kaua'i [*Moore et al.*, 1989]. There is no evidence of significant landsliding on the west end of Ka'ena Ridge.

[7] Ka'ena Ridge is an elongate, relatively flat-topped submerged terrace 35–55 km wide that extends ~80 km from the western edge of O'ahu. The terrace is bounded by a break in slope that marks a paleoshoreline (1200–1500 m on the north side of Ka'ena Ridge and ~1400 m deep on the south side [*Coombs et al.*, 2004]). Two submarine shields, 15 km and 10 km in diameter, rise 200 m above the western part of Ka'ena Ridge and to within 660–880 m of sea level (approximately 2500 m above the basal seafloor) [*Smith*, 2002]. A submarine rift zone called Waialu Ridge extends northwest from Ka'ena Ridge (Figure 1). There are few circular flat-topped cones closer to Kaua'i; radiating ridges with elongate sediment-filled basins and submarine canyons and channels are more common within ~20 km of Kaua'i. Young lava flows were recognized southwest of Ka'ena Ridge by *Holcomb and Robinson* [2004] from GLORIA side-scan sonar imagery, but there has been no previous study of the submarine features between Kaua'i and O'ahu. In 2007, three dives using the remotely operated vehicle (ROV) *Jason*2 from Woods Hole Oceanographic Institution aboard R/V *Kilo Moana* were conducted to survey and sample the volcanic cones and lava flows west of Ka'ena Ridge for petrologic, geochronological, and geochemical studies [*Garcia et al.*, 2008]. In 2009, a

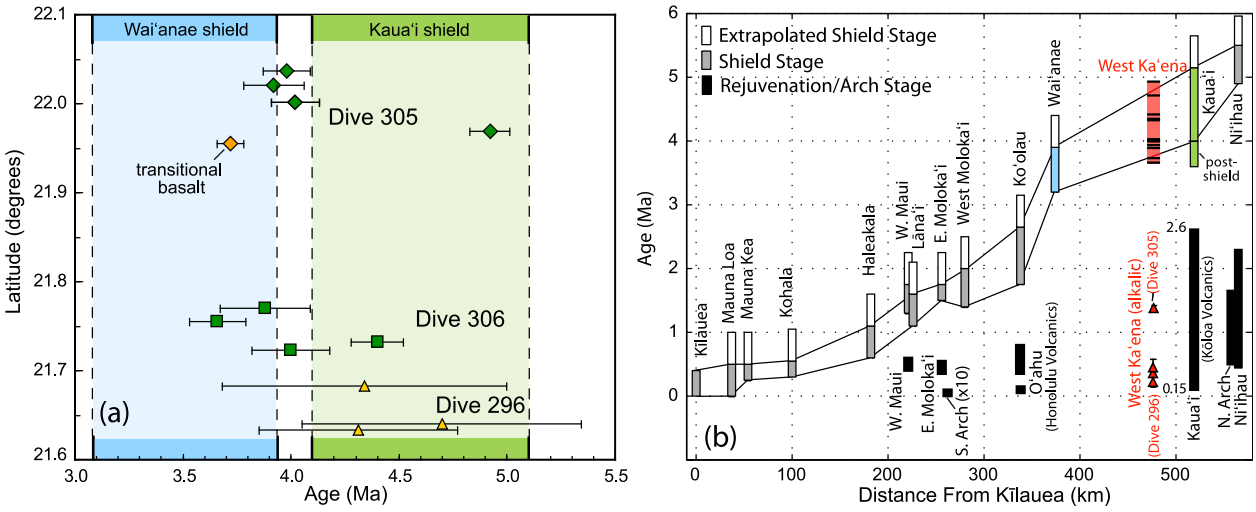

Figure 3. (a) Latitude versus age (Ma) of West Ka'ena lavas. Green symbols are Ar-Ar ages, and yellow symbols are K-Ar ages. (b) Age (Ma) versus distance from Kīlauea volcano (km) for shield and rejuvenated volcanism for the Hawaiian Islands. Postshield ages are shown for Kaua'i. Data from *Bianco et al.* [2005], *Tagami et al.* [2003], and *Ozawa et al.* [2005] with new Kōloa ages from *Hearty et al.* [2005], *Sano* [2006], and *Garcia et al.* [2010]. Error bars in Figure 3a are $\pm 2\sigma$, shown in Table 1. Age ranges for Kaua'i and Wai'anae volcanoes are shown by colored fields in Figure 3a. Tick marks within vertical red bar in Figure 3b show ages of West Ka'ena samples from this study from Figure 3a and Table 1. Black bars represent secondary volcanism, gray bars represent shield volcanism, and white bars represent extrapolated shield stage (uniformly 500 ka to estimate the duration of shield volcanism). Symbols for West Ka'ena lavas are as follows: Dive 306 (squares), Dive 305 (diamonds), and Dive 296 (triangles).

single dredge haul was collected ~30 km northeast of Kaua'i (Figure 1).

3. Description of Dive Areas and Petrology of Samples

[8] From north to south, the three dives covered a distance spanning ~70 km. Dive 305 traversed an elongate cluster of flat-topped and conical seamounts extending northwest from the end of Ka'ena Ridge (Figure 2a; auxiliary material).[1] These cones are <200 m high and <0.4–2 km in diameter with summits at depths of 2700 to 3500 m. Dive 306 sampled 6 cones in a cluster southwest of the end of Ka'ena Ridge and a terrace and cone at the base of the end of Ka'ena Ridge. Several cones are disc-shaped, flat-topped cones with steep flanks (~20–30°) and basalt diameters between 1 and 3 km, similar to cones described by *Clague et al.* [2000]. The cones consist predominantly of pillowed flows and mounds. Thin sheet flows are also present on some of the cones. Dive 296 was 20 km south of the Dive 306 area, over several cone clusters and three young lava fields with high sonar backscatter compared to the surrounding seafloor (Figure 2b). These flows are at water depths greater than 4300 m. The largest flow, 22 km long and 7 km across at its widest point, was previously mapped as a young flow [*Holcomb and Robinson*, 2004]. The western, higher-elevation portion of this field appears to emanate from the base of a preexisting submarine tholeiitic cone. A total of 89 samples were collected during Dives 296, 305, and 306 and the dredge haul (sample locations and descriptions are included in the auxiliary material). Sixty-nine of these samples are basalt or volcanic breccia; eighteen samples are sedimentary rocks (primarily biogenic mudstones and several volcaniclastic rocks collected on the cones).

[9] West Ka'ena lavas are mostly olivine basalt that display cryptocrystalline or intersertal textures with variable amounts of olivine phenocrysts and vesicles. Euhedral to subhedral olivine phenocrysts (<5 mm) make up 5 to 20 vol % of almost all of the lavas and xenocrysts are rare. Chromite inclusions are typically found in the olivine phenocrysts. Clinopyroxene are less common and occurs mostly as microphenocrysts (<1 mm, <5 vol %). The lava groundmass consists of variable amounts of clinopyroxene, olivine, plagioclase, Fe-Ti oxides, cryptocrystalline material, and devitrified glass. The lavas typically contain <1 vol % vesicles, but several

[1]Auxiliary material data sets are available at ftp://ftp.agu.org/apend/gc/2010gc003233. Other auxiliary materials are in the HTML.

Table 1. Summary of Whole-Rock Plateau and Isochron Ages for West Ka'ena Ridge Lavas[a]

Sample	Group	Location	Total Fusion Age (Ma) ± 2σ	Isochron Analysis			N	Age Spectrum (Plateau) Analysis		
				$^{40}Ar/^{36}Ar_i$ ± 2σ	MSWD	Age (Ma) ± 2σ		^{39}Ar %	MSWD	Age (Ma) ± 2σ
					Dive 296					
296-20	alk	Cone D	0.393 ± 0.058	296.0 ± 1.9	0.15	0.363 ± 0.102	8 of 8	100.0	0.18	0.389 ± 0.048
			0.322 ± 0.059	295.0 ± 0.9	0.74	0.384 ± 0.057	9 of 9	97.7	0.81	0.360 ± 0.039
										0.371 ± 0.040[b]
					Dive 305					
305-02	alk	Cone A	1.38 ± 0.05	287.7 ± 11.4	0.33	1.47 ± 0.13	8 of 8	100.0	0.54	**1.39 ± 0.05**
305-04	thol	Cone B	3.94 ± 0.13	298.8 ± 8.8	0.53	3.91 ± 0.22	8 of 8	100.0	0.54	**3.98 ± 0.11**
305-07	thol	Ledge C	3.96 ± 0.21	298.3 ± 7.0	0.38	3.89 ± 0.18	8 of 8	100.0	0.42	**3.93 ± 0.15**
305-14	thol	Cone E	4.10 ± 0.18	297.9 ± 2.2	1.01	3.75 ± 0.32	8 of 8	100.0	1.49	4.05 ± 0.19
			4.14 ± 0.21	297.6 ± 2.1	0.24	3.76 ± 0.30	8 of 8	100.0	0.74	4.10 ± 0.14
										4.02 ± 0.11[b]
305-20	thol	Cone G	4.87 ± 0.12	295.6 ± 7.3	1.08	4.92 ± 0.13	8 of 8	100.0	0.94	**4.92 ± 0.09**
305-24	trans	Cone H	3.85 ± 0.08	300.1 ± 58.8	0.44	3.63 ± 0.63	6 of 10	71.7	0.36	3.68 ± 0.07
			3.89 ± 0.12	331.2 ± 43.6	0.61	3.44 ± 0.45	5 of 10	78.2	0.98	3.80 ± 0.11
										3.72 ± 0.06[b]
					Dive 306					
306-03	thol	Cone A	4.00 ± 0.26	298.2 ± 6.6	0.10	3.49 ± 1.16	10 of 10	100.0	0.17	3.98 ± 0.24
			3.40 ± 1.63	299.2 ± 10.2	0.31	3.40 ± 1.63	8 of 8	100.0	0.34	4.01 ± 0.28
										4.00 ± 0.18[b]
306-05	thol	Cone B	4.38 ± 0.15	294.4 ± 4.7	0.82	4.42 ± 0.15	8 of 8	100.0	0.72	**4.40 ± 0.12**
306-15	thol	Cone D	3.61 ± 0.25	297.9 ± 3.8	0.95	3.52 ± 0.24	10 of 10	100.0	1.02	3.62 ± 0.19
			3.67 ± 0.24	294.7 ± 7.1	0.33	3.73 ± 0.37	7 of 7	100.0	0.28	3.69 ± 0.18
										3.66 ± 0.13[b]
306-31	thol	Cone I	3.81 ± 0.41	291.5 ± 12.0	0.22	4.13 ± 0.82	10 of 10	100.0	0.24	3.87 ± 0.31
			4.16 ± 0.23	282.9 ± 33.3	0.38	4.56 ± 1.78	5 of 8	62.2	0.42	3.88 ± 0.28
										3.88 ± 0.21[b]

[a]Group is based on geochemistry: alk, alkalic basalt; thol, tholeiitic basalt; trans, transitional basalt. Bold age is preferred age, with error reported for ±2σ. MSWD refers to mean sum of the weighted deviates, which is a measure of the scatter compared to that which is expected from analytical uncertainties. Percentage of ^{39}Ar degassed used in the plateau calculation. N is number of steps included in the plateau calculation. Analytical methods are described in Appendix A.

[b]Weighted mean plateau age from two experiments.

Table 2. Major Element and Trace Element Abundances in Whole-Rock Samples of West Ka'ena Ridge Lavas[a]

	Sample									
	296-25	296-26	305-04	305-07	306-27	306-30	305-24	306-19	296-22	305-02
Group	thol basalt	thol basalt	thol basalt	thol basalt	thol basalt	thol basalt	trans basalt	trans basalt	alk basalt	alk basalt
Area	Cone E	Cone F	Cone B	Ledge C	Cone F	Cone H	Cone H	Cone E	Cone D	Cone A
Latitude (deg)	21.641	21.644	22.037	22.021	21.755	21.770	21.955	21.757	21.635	22.049
Longitude (deg)	159.041	159.043	158.920	158.904	158.992	158.957	158.888	159.007	159.040	158.924
Unnormalized Major Element Oxides (wt %)										
SiO_2	50.55	49.17	51.74	50.22	51.32	50.23	48.98	50.03	45.15	41.67
TiO_2	2.48	2.63	1.71	1.95	1.46	1.98	2.75	2.68	2.75	2.34
Al_2O_3	13.29	11.47	12.62	12.22	11.82	12.01	13.43	13.71	14.03	10.72
Fe_2O_3*	12.00	13.64	11.31	12.07	11.26	12.58	12.43	12.10	13.27	14.40
MnO	0.18	0.20	0.17	0.19	0.17	0.18	0.21	0.16	0.20	0.21
MgO	7.90	11.44	10.78	11.45	13.10	11.54	9.03	8.58	6.16	13.85
CaO	10.57	8.62	8.87	8.83	8.57	9.44	9.11	8.59	12.40	12.05
Na_2O	2.19	2.27	2.26	2.18	1.94	1.85	2.81	2.87	3.16	3.03
K_2O	0.46	0.48	0.58	0.51	0.28	0.29	1.15	0.95	2.07	0.86
P_2O_5	0.25	0.28	0.22	0.23	0.15	0.18	0.46	0.47	0.53	0.64
Total	99.88	100.20	100.26	99.86	100.07	100.28	100.36	100.14	99.72	99.77
LOI	−0.07	0.08	0.43	0.32	−0.47	0.74	0.33	0.66	2.45	0.67
Trace Elements (ppm)										
La	12.9	12.7	10.4	9.8	5.7	6.2	24.4	21.4	28.2	43.9
Ce	28.8	29.7	24.0	23.8	14.6	16.1	51.8	48.0	58.0	89.4
Pr	4.08	4.19	3.32	3.35	2.03	2.40	6.92	6.56	7.09	10.4
Nd	19.1	20.2	15.6	16.1	10.1	12.0	32.8	32.0	30.2	41.3
Sm	4.97	5.53	4.12	4.55	2.91	3.62	7.59	7.87	6.71	8.59
Eu	1.60	1.74	1.30	1.55	1.04	1.25	2.28	2.42	2.11	2.73
Gd	5.12	5.60	3.97	4.79	3.17	4.09	6.73	7.39	6.32	7.51
Tb	0.77	0.89	0.69	0.71	0.48	0.71	1.01	1.00	0.88	0.96
Dy	4.85	4.99	3.98	4.30	2.95	4.25	5.54	5.84	5.12	5.09
Ho	0.83	0.94	0.73	0.81	0.57	0.77	0.96	0.99	0.84	0.88
Er	2.20	2.52	2.11	2.09	1.47	2.15	2.43	2.44	2.14	2.03
Yb	1.83	2.05	1.78	1.69	1.30	1.78	1.98	1.95	1.70	1.42
Lu	0.21	0.28	0.25	0.24	0.18	0.25	0.26	0.29	0.19	0.21
V	269	260	228	217	197	242	244	233	285	254
Cr	369	581	588	634	789	857	422	335	72	546
Ni	131	435	332	435	465	413	243	254	68	394
Zn	114	133	106	121	105	135	136	143	130	129
Ga	20	18	17	17	15	17	21	21	22	18
Rb	6.7	7.3	7.3	6.3	4.0	3.8	19.3	14.4	29.3	17.3
Sr	341	301	279	326	213	206	568	525	701	722
Y	24.0	26.1	21.7	22.4	17.0	22.0	26.6	27.3	24.5	23.1
Zr	141	160	121	126	83	100	227	234	148	162
Nb	13.5	14.0	9.1	9.2	5.9	7.7	24.0	18.4	46.9	58.5
Cs		0.07	0.08	0.07	0.03	0.05	0.20	0.16	0.39	0.19
Ba	90	83	91	74	46	47	221	187	560	722
Hf	2.64	3.88	2.85	2.92	1.78	2.48	5.05	5.00	2.61	3.58
Ta	0.52	0.81	1.57	1.00	0.27	0.89	1.67	1.19	1.66	3.33
Pb	0.96	1.01	1.37	0.92	0.60	0.64	2.89	2.04	1.72	2.56
Th	0.71	0.88	0.66	0.62	0.29	0.35	1.62	1.36	3.20	5.52
U	0.21	0.22	0.19	0.18	0.10	0.13	0.51	0.41	0.83	1.26

[a]See Data Set S1 in the auxiliary material for complete data. Abbreviations for groups are as follows: thol basalt, tholeiitic basalt; trans basalt, transitional basalt; alk basalt, alkalic basalt. XRF analyses were performed at University of Massachusetts XRF Laboratory. Fe_2O_3* is total iron expressed as Fe_2O_3. LOI is loss on ignition. Totals have not been resummed using the LOI value. Elements by XRF are as follows: V, Cr, Ni, Zn, Ga, Rb, Sr, Y, Zr, Nb, and Ba. ICP-MS analyses were performed at the PCIGR at University of British Columbia. Elements by ICP-MS are as follows: REE, Cs, Hf, Ta, Pb, Th, and U. Analytical methods are described in Appendix A.

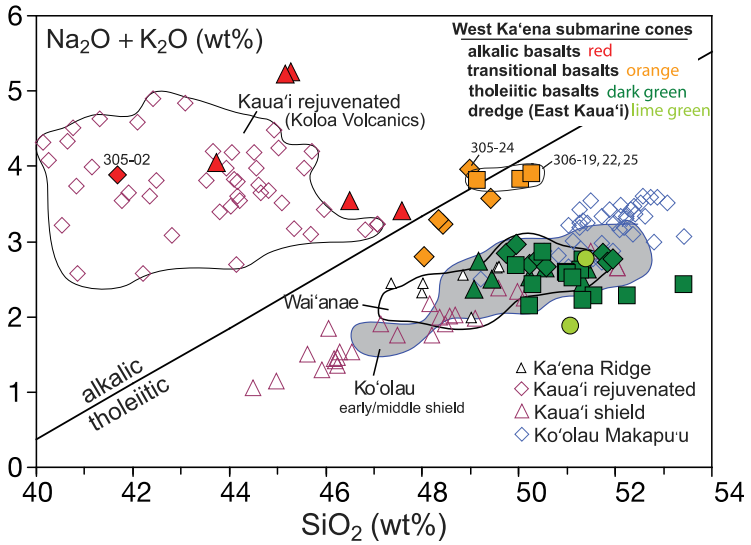

Figure 4. Total alkalis versus silica variation diagram for whole-rock samples from West Ka'ena submarine cones. Alkalic-tholeiitic boundary from *MacDonald and Katsura* [1964]. "Kaua'i" late shield and rejuvenated (Kōloa Volcanics) data from *Garcia et al.* [2010]. Wai'anae shield field (black outline) based on data from *MacDonald and Katsura* [1964] and *Sherrod et al.* [2007]. Kaua'i shield data from *Mukhopadhyay et al.* [2003]. Ko'olau early middle shield field (blue curve) from *Haskins and Garcia* [2004]; Ko'olau late shield data (Makapu'u stage) from *Frey et al.* [1994]. Ka'ena Ridge data from *Coombs et al.* [2004]. Three transitional basalts from Dive 306 (Cone E; 306-19, 306-22, and 306-25) are highly vesicular and have the high alkali contents. Dive 305-24 is highly altered and falls slightly above the alkalic-tholeiitic divide but has similar trace element and isotopic composition to the transitional basalts. Symbols for West Ka'ena lavas are as follows: Dive 306 (squares), Dive 305 (diamonds), and Dive 296 (triangles).

samples have >10 vol % small, round vesicles. The lavas have weak to moderate levels of alteration. The secondary minerals include iddingsite partially replacing olivine, clay partly replacing glassy and cryptocrystalline material, and zeolites and calcite infilling some vesicles.

4. Age of West Ka'ena Lavas

[10] Eleven samples from Dives 296, 305 and 306 were dated using the Ar-Ar method (Table 1); six samples from Dive 296 (4 tholeiitic, 2 alkalic) were dated by the K-Ar technique (auxiliary material; see Appendix A for analytical methods). Seven of the eleven lavas (tholeiitic basalts, and one transitional basalt) from Dives 305 and 306 range in age from 4.00 ± 0.18 to 3.66 ± 0.13 Ma (Figure 3a and Table 1; all errors are ±2σ). Two additional samples have Ar-Ar ages of 4.40 ± 0.12 and 4.92 ± 0.09 Ma. Six duplicate measurements yielded reproducible ages within analytical error and the total fusion ages for all samples match the plateau ages within error. The plateau ages of these samples represent a high percentage of the ^{39}Ar (100% for 13 of 17 analyses) and have low MSWD values (Table 1). Three of the four unaltered tholeiitic basalts from Dive 296 dated by the K-Ar method range in age from 4.70 ± 0.64 to 4.31 ± 0.46 Ma (auxiliary material). The K-Ar age for the fourth sample (296-30) is 2.85 ± 1.08 Ma. A higher LOI value of 0.84 wt % and air contamination of 94.1% for this sample indicate Ar loss, therefore the obtained age is likely younger than the real age. The Ar-Ar and K-Ar ages for West Ka'ena lavas overlap and fall between the current estimates for the age of shield stage volcanism on Kaua'i (5.1–4.0 Ma [*Garcia et al.*, 2010]) and Wai'anae volcano (3.9–3.1 Ma [*Guillou et al.*, 2000]) on O'ahu (Figures 3a and 3b). There is no apparent relationship between cone location and age, except that the three K-Ar ages for Dive 296 lavas are slightly older than the average Ar-Ar age for Dives 305 and 306 to the north.

[11] Two alkalic samples, one collected from a cone adjacent to the large young lava flow from Dive 296 (296-20; Figure 2) and one from Dive 305 (305-02), yielded Ar-Ar ages of 0.37 ± 0.04 and 1.39 ± 0.05 Ma, respectively (Figure 3b and Table 1). Mass fractionation corrected K-Ar ages for two samples from the young lava flow from Dive 296 (296-20, 296-21) are 0.24 ± 0.16 and 0.47 ± 0.24 Ma (see Appendix A and auxiliary

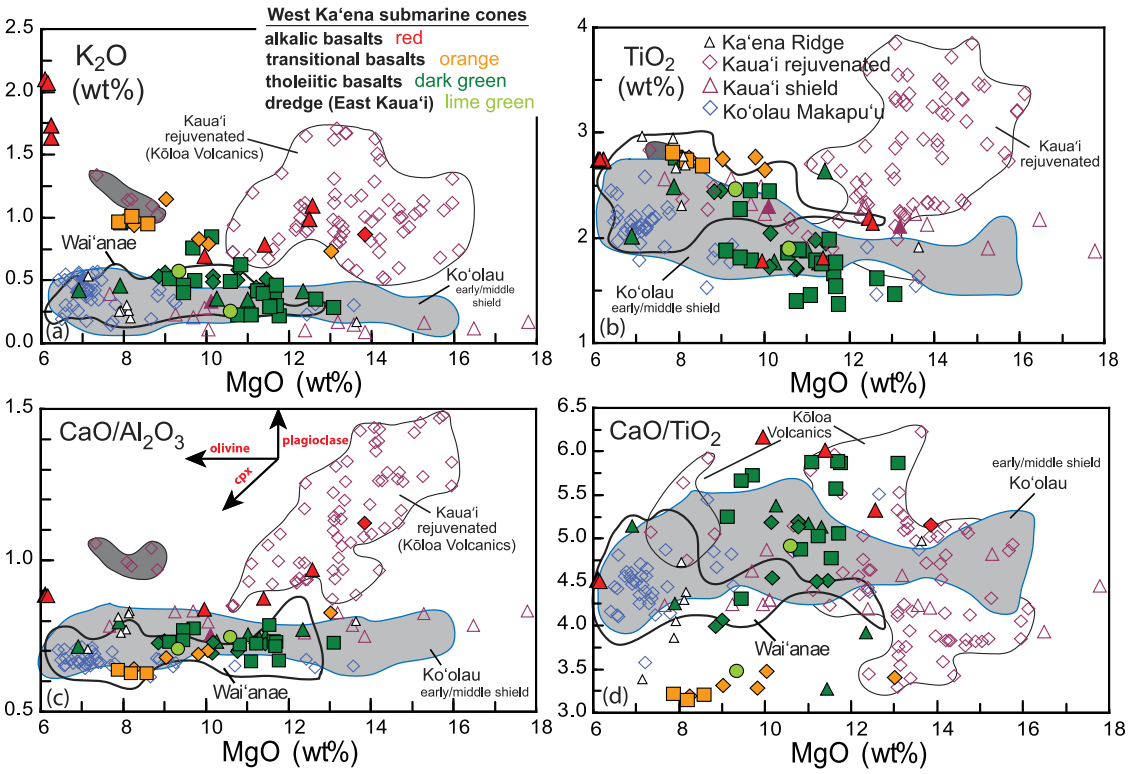

Figure 5. Whole-rock major element variation diagrams for West Ka'ena lavas. (a) K_2O versus MgO. (b) TiO_2 versus MgO. (c) CaO/Al_2O_3 versus MgO. (d) CaO/TiO_2 versus MgO. Data sources listed in Figure 4. Symbols for West Ka'ena lavas are the same as in Figure 4.

material). The ages for these alkalic lavas overlap current estimates for the age of rejuvenated volcanism on Kaua'i (2.6–0.15 Ma [*Garcia et al.*, 2010]) and O'ahu (0.80–0.1 Ma [*Ozawa et al.*, 2005]) (Figure 3b).

5. Whole-Rock Chemistry

5.1. Major and Trace Element Compositions

[12] Most of the analyzed lavas (38 of 52) from cones west of Ka'ena Ridge are tholeiitic basalts with large ranges in MgO (7–13 wt %) and SiO_2 (49–53 wt %) (Table 2; see Appendix A for analytical methods). Eight lavas from Dives 305 and 306 are transitional basalts with 48–50 wt % SiO_2, 8–13 wt % MgO, and 3–4 wt % $Na_2O + K_2O$ that plot near the alkalic-tholeiitic boundary (Figures 4 and 5). Of the tholeiitic and transitional basalts, 15 samples have >51 wt % SiO_2 (referred to as high-SiO_2 lavas). Six lavas are alkalic basalts with 42–48 wt % SiO_2, 10–14 wt % MgO, and 3.5–5.3 wt % $Na_2O + K_2O$, similar in composition to rejuvenated lavas from Kaua'i (3 of the 6 alkalic basalts are from flows <0.5 Ma in age, sampled during Dive 296, except 305-02 is from the most northerly cone from Dive 305).

[13] The tholeiitic basalts form a broad compositional field in which K_2O mostly increases and CaO/Al_2O_3 (0.6–0.8) shows a narrow range with decreasing MgO (Figure 5). All but two of the tholeiitic lavas have >9 wt % MgO, so they are not likely to show inflections in CaO/Al_2O_3 as a result of clinopyroxene and plagioclase fractionation. The transitional basalts have higher TiO_2 (2.7–2.8 wt %) and lower CaO/TiO_2 than most tholeiitic basalts (1.3–2.6 wt % TiO_2). The trace element abundances of the tholeiitic basalts (La/Sm_N = 1.0–1.6; Dy/Yb_N = 1.4–1.7) are lower than the transitional basalts (La/Sm_N = 1.7–2.1 Dy/Yb_N = 1.8–2.0) except for the heavy rare earth elements (HREE; Figure 6a). There are only a few crossing REE patterns. One transitional basalt and one alkalic basalt also show different variations in Pb and K than other West Ka'ena lavas. The alkalic basalts are highly enriched in incompatible trace elements. Almost all the tholeiitic, transitional, and alkalic basalts are depleted in Cs, Th and U relative to Ba and K, and in Pb relative to Ce and Pr. Hf in 6 of 15

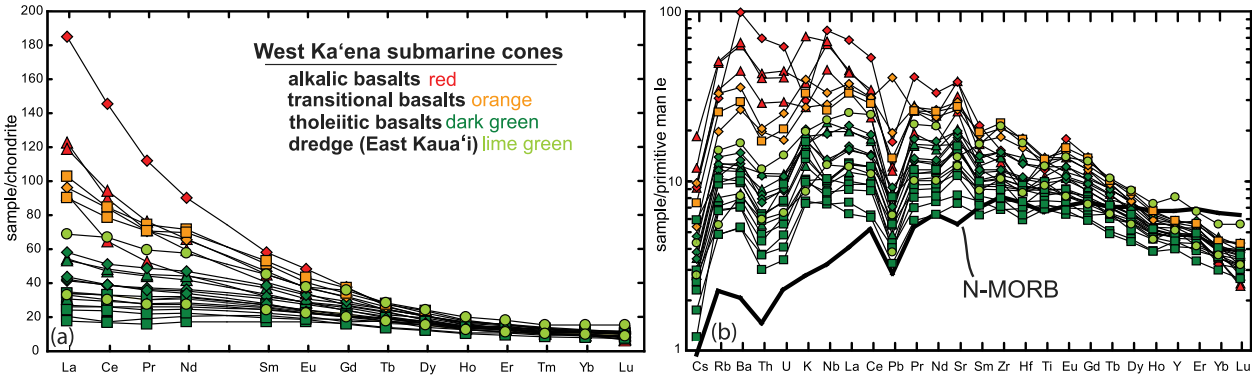

Figure 6. Whole-rock REE and other incompatible element concentrations for West Ka'ena lavas. Normalization values are from *McDonough and Sun* [1995]. NMORB average from *Salters and Stracke* [2004]. Symbols are the same as in Figure 4.

analyzed tholeiitic lavas shows depletion relative to Ti and Zr in primitive mantle-normalized trace element patterns (Figure 6b).

[14] In addition to distinguishing among the tholeiitic, transitional, and alkali basalts, the trace element ratios also reveal melting relationships and source differences between the different types of basalts. The tholeiitic basalts have similar Nb/Y and Zr/Y to Hawaiian shield stage lavas and the transitional basalts have slightly higher ratios

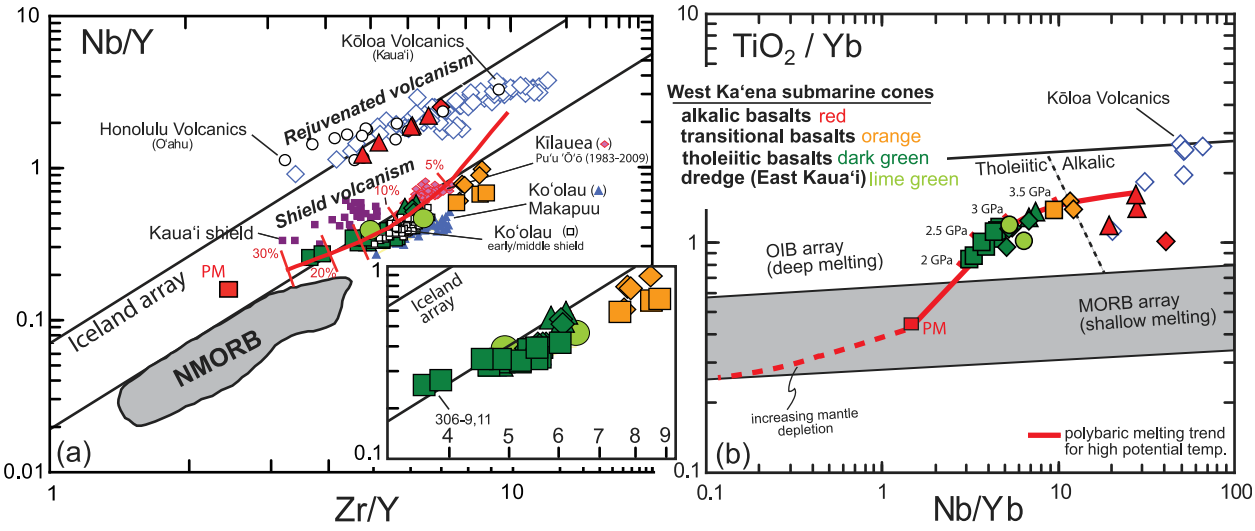

Figure 7. Whole-rock trace element ratio variation diagrams for West Ka'ena lavas. (a) Nb/Y versus Zr/Y. Plot originated from *Fitton et al.* [1997]. (b) TiO_2/Yb versus Nb/Yb. Plot, fields, and melt model originated from *Pearce* [2008]. Melting model shown in Figure 7a with red curve marked with percent melting is for tholeiitic basalts, not alkalic basalts. The model assumes incongruent dynamic melting [*Zou and Reid*, 2001] and coefficients for melting reactions based on lherzolite melting experiments [e.g., *Kinzler and Grove*, 1992; *Walter*, 1998; *Longhi*, 2002]. The model simulates garnet lherzolite melting because garnet is required in the source to produce variations of HREE observed in West Ka'ena lavas. One percent of the total residue is residual melt. Partition coefficients from *Salters and Stracke* [2004] and *Shaw* [2000] were kept constant. Source mineralogy for primitive mantle garnet lherzolite is 0.2cpx:0.25opx:0.5ol:0.05gt. Data sources for Figure 7a are as follows: Kōloa Volcanics [*Garcia et al.*, 2010], Honolulu Volcanics [*Yang et al.*, 2003], Ko'olau Makapu'u [*Frey et al.*, 1994], Ko'olau shield Kalihi stage [*Haskins and Garcia*, 2004], Kaua'i shield [*Mukhopadhyay et al.*, 2003], and Kīlauea-Pu'u 'Ō'ō [*Garcia et al.*, 1992, 1996, 2000]. PM, primitive mantle. PM composition from *McDonough and Sun* [1995]. Parameters for melting model shown in Figure 7b are described by *Pearce* [2008]. Estimates for degree of partial melting for HSDP lavas range from 8% to 15% [*Feigenson et al.*, 2003]. Inset in Figure 7a shows only lavas from west of Ka'ena Ridge.

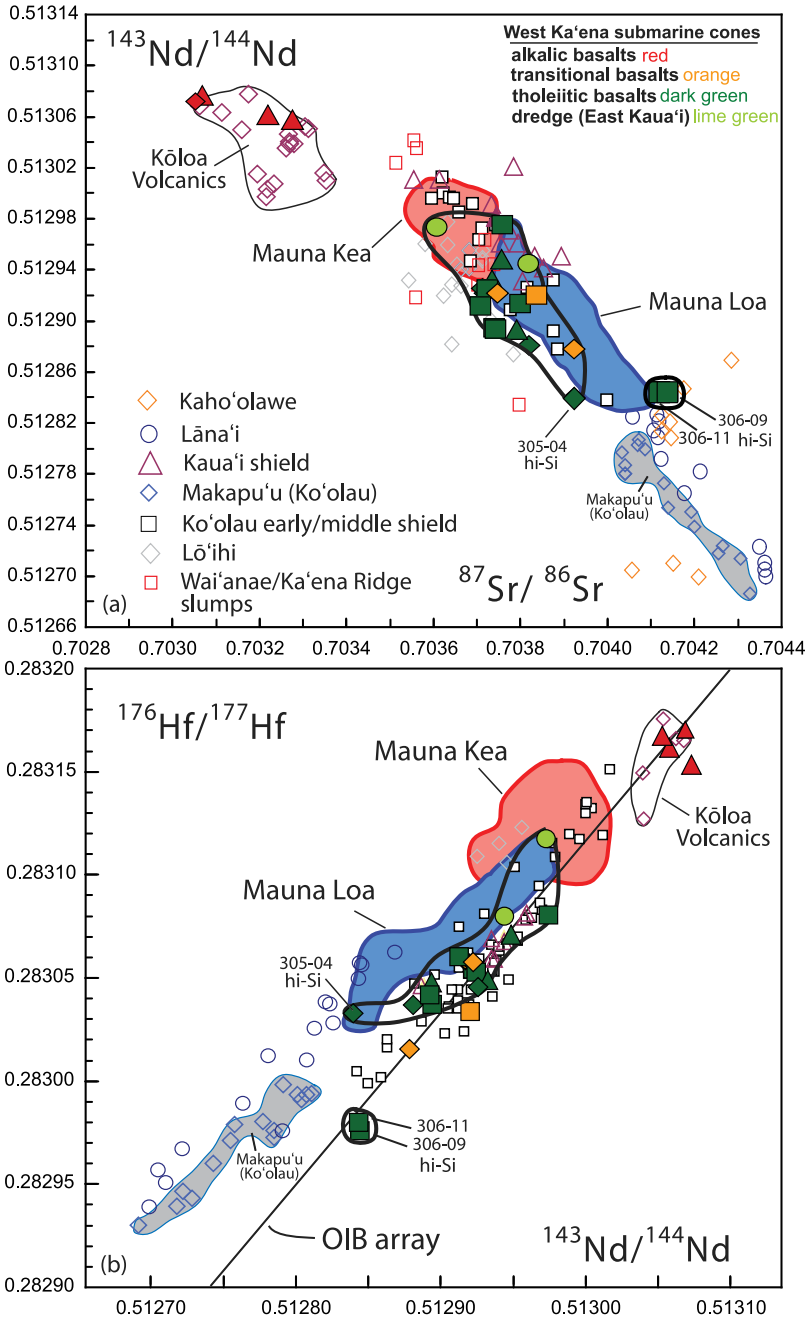

Figure 8. Sr-Nd-Hf isotopic compositions for West Ka'ena lavas compared to other Hawaiian shield volcanoes. (a) Plot of $^{143}Nd/^{144}Nd$ versus $^{87}Sr/^{86}Sr$. (b) Plot of $^{176}Hf/^{177}Hf$ versus $^{143}Nd/^{144}Nd$. References for data sources are listed in the auxiliary material (Text S1). All isotope data from Hawaiian shield volcanoes are normalized to the same set of standards. Ocean island basalt (OIB) array from *Vervoort et al.* [1999]. West Ka'ena lavas are outlined with black circles.

(Figure 7a). The tholeiitic and transitional lavas overlap shield lavas from Hawaiian Islands and form a trend that corresponds with an incongruent dynamic melting model (Figure 7a). The alkalic basalts overlap rejuvenated lavas from Kaua'i and O'ahu. In a plot of TiO_2/Yb versus Nb/Yb [e.g., *Pearce*, 2008], the tholeiitic and transitional basalts lie along a predicted melting trend, with the transitional basalts indicating deeper, lower-degree melting than the tholeiitic basalts (Figure 7b). The tholeiitic and transitional basalts have overlapping Nb/La (not shown).

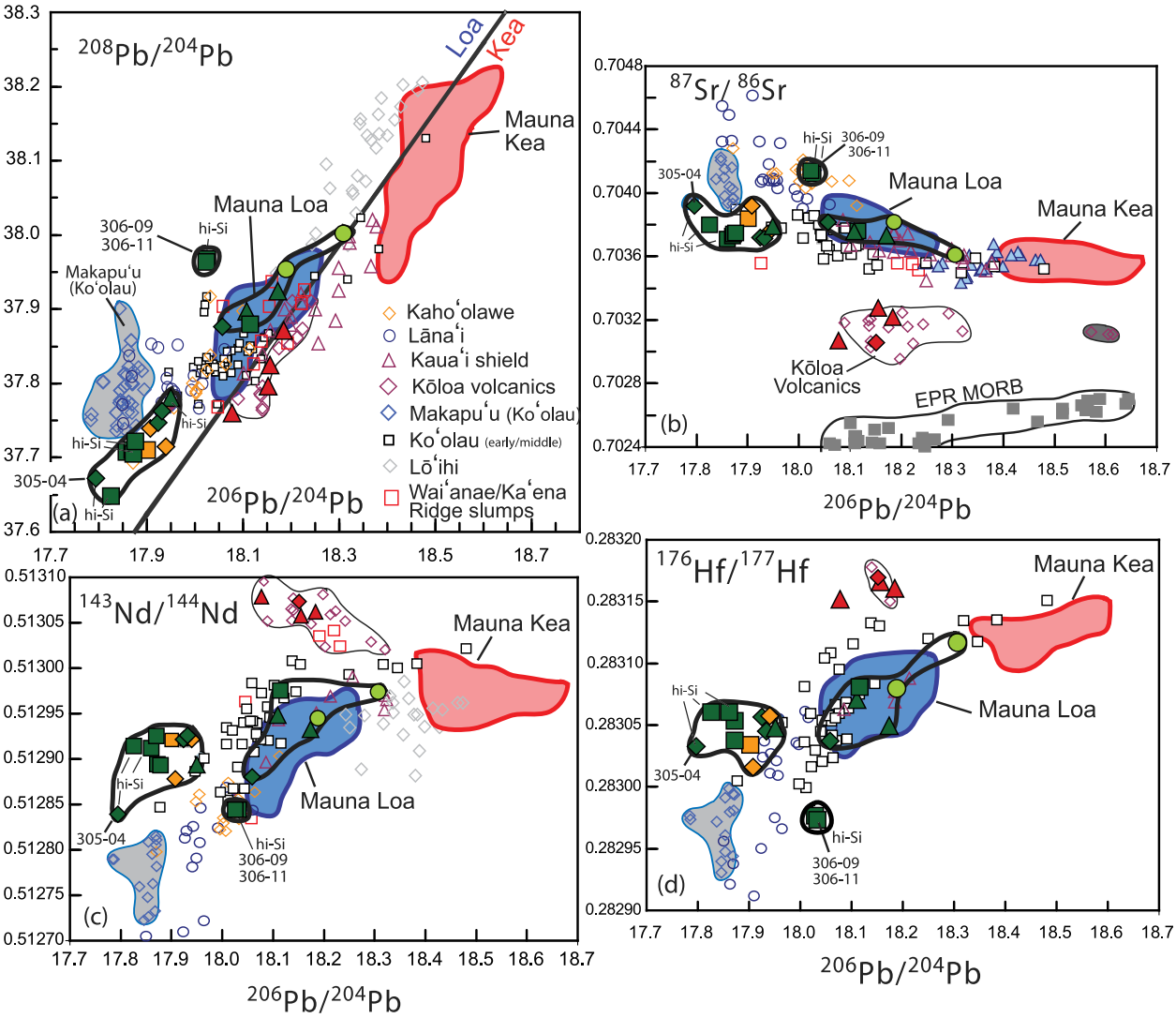

Figure 9. Sr-Nd-Hf-Pb isotopic compositions for West Ka'ena lavas compared to other Hawaiian shield volcanoes. (a) Plot of $^{208}Pb/^{204}Pb$ versus $^{206}Pb/^{204}Pb$. (b) Plot of $^{87}Sr/^{86}Sr$ versus $^{206}Pb/^{204}Pb$. (c) Plot of $^{143}Nd/^{144}Nd$ versus $^{206}Pb/^{204}Pb$. (d) Plot of $^{176}Hf/^{177}Hf$ versus $^{206}Pb/^{204}Pb$. References for data sources are listed in the auxiliary material (Text S1). Bold line in Figure 9a marks the Loa-Kea divide from *Abouchami et al.* [2005]. All isotope data from Hawaiian shield volcanoes are normalized to the same set of standards. West Ka'ena lavas are outlined with black circles.

5.2. Sr-Nd-Hf-Pb Isotopic Compositions

[15] Tholeiitic and transitional basalts from submarine cones west of Ka'ena Ridge have overlapping Sr, Nd, Hf, and Pb isotopic compositions that are significantly different from those of the alkalic basalts (Figures 8 and 9; see Appendix A for analytical methods). Except for three anomalous lavas with high SiO_2 (305-04, 306-09, 306-11), the tholeiitic and transitional basalts have a restricted range of Sr, Nd, and Hf isotopic compositions ($^{87}Sr/^{86}Sr$ = 0.70373–0.70393; $^{143}Nd/^{144}Nd$ = 0.51284–0.51297; $^{176}Hf/^{177}Hf$ = 0.28303–0.28308; Table 3 and Figure 8). Pb isotopic compositions of the tholeiitic and transitional lavas span a greater compositional range than Sr, Nd, and Hf, relative to the whole isotopic range of Hawaiian lavas, and form two groups (except for 306-09 and 306-11); one group clusters at intermediate Pb isotopic compositions and overlaps with the Mauna Loa field, and the other group extends to very low $^{208}Pb/^{204}Pb$ and $^{206}Pb/^{204}Pb$ (Figure 9). The two samples (306-09 and 306-11, having high-SiO_2, low CaO and K_2O, and low Zr/Y) that lie away from the two main groups have also lower Hf and Nd and higher Sr isotopic compositions, and higher $^{208}Pb/^{204}Pb$ with respect to $^{206}Pb/^{204}Pb$. Sample

Table 3. Sr, Nd, Hf, and Pb Isotopic Geochemistry of Whole-Rock Samples of West Ka'ena Lavas[a]

Sample	$^{87}Sr/^{86}Sr$	2SE	$^{143}Nd/^{144}Nd$	2SE	ε_{Nd}	$^{176}Hf/^{177}Hf$	2SE	ε_{Hf}	$^{206}Pb/^{204}Pb$	2SE	$^{207}Pb/^{204}Pb$	2SE	$^{208}Pb/^{204}Pb$	2SE
Tholeiitic Basalts														
296-25	0.703733	8	0.512949	7	6.1	0.283049	9	9.8	18.1722	4	15.4658	8	37.923	20
296-26	0.703755	9	0.512932	4	5.7	0.283071	5	10.6	18.1086	5	15.4542	10	37.896	24
296-32	0.703788	9	0.512893	5	5.0	0.283048	6	9.8	17.9496	5	15.4525	10	37.780	26
296-32 dup	0.703795	9	0.512904	5	5.2	0.283039	5	9.4	17.9481	6	15.4528	12	37.781	31
305-04	0.703920	8	0.512840	6	3.9	0.283033	6	9.2	17.7954	10	15.4361	7	37.671	25
305-04 dup	0.703926	9	0.512862	7	4.4	0.283040	15	9.5	17.7968	8	15.4377	7	37.675	17
305-07	0.703716	8	0.512922	5	5.5	0.283057	3	10.1	17.9242	8	15.4483	7	37.747	16
305-09	0.703710	8	0.512926	7	5.6	0.283046	5	9.7	17.9323	7	15.4512	8	37.762	15
305-14	0.703816	9	0.512881	8	4.7	0.283037	4	9.4	18.0572	7	15.4550	6	37.876	19
306-01	0.703709	9	0.512911	6	5.3	0.283061	4	10.2	17.8603	8	15.4424	7	37.706	19
306-05	0.703723	8	0.512925	6	5.6	0.283053	4	9.9	17.8718	7	15.4427	7	37.709	18
306-09	0.704119	8	0.512844	6	4.0	0.282976	6	7.2	18.0279	7	15.4480	6	37.966	21
306-11	0.704137	10	0.512844	6	4.0	0.282980	6	7.4	18.0255	19	15.4577	24	37.963	77
306-15	0.703798	8	0.512913	8	5.4	0.283060	6	10.2	17.8267	6	15.4412	6	37.647	16
306-26	0.703740	7	0.512894	7	5.0	0.283037	5	9.4	17.8727	7	15.4398	8	37.704	19
306-27	0.703743	8	0.512893	8	5.0	0.283042	5	9.5	17.8785	21	15.4516	22	37.720	65
306-30	0.703759	8	0.512975	6	6.6	0.283080	5	10.9	18.1155	7	15.4504	6	37.878	19
EK-1	0.703607	8	0.512973	8	6.5	0.283117	4	12.2	18.3074	8	15.4680	7	38.002	23
EK-2	0.703816	8	0.512944	9	6.0	0.283079	6	10.9	18.1885	9	15.4570	9	37.953	27
Transitional Basalts														
305-20	0.703920	7	0.512878	6	4.7	0.283016	6	8.6	17.9075	6	15.4455	6	37.738	17
305-24	0.703744	9	0.512922	6	5.5	0.283058	5	10.1	17.9396	8	15.4534	7	37.714	17
306-19	0.703837	8	0.512920	6	5.5	0.283033	6	9.2	17.9018	6	15.4447	5	37.709	15
Alkalic Basalts														
296-01	0.703220	8	0.513062	7	8.3	0.283161	5	13.8	18.1844	5	15.4561	9	37.871	27
296-11	0.703071	8	0.513077	6	8.6	0.283153	4	13.5	18.0771	8	15.4345	7	37.759	20
296-22	0.703276	10	0.513058	6	8.2	0.283167	5	14.0	18.1557	14	15.4559	13	37.824	37
305-02	0.703054	9	0.513073	5	8.5	0.283170	5	14.1	18.1519	7	15.4472	7	37.796	19

[a]Abbreviations are as follows: thol, tholeiitic basalt; trans, transitional basalt; alk, alkalic basalt. dup indicates complete chemistry duplicate. All trace element and isotopic analyses were carried out at the PCIGR. The analytical methods are described in Appendix A. Two SE (standard error) is expressed as 106 for Sr, Nd, and Hf and times 104 for Pb.

305-04 extends to the lowest $^{206}Pb/^{204}Pb$ and $^{143}Nd/^{144}Nd$, and is the only sample displaced significantly above the Hf-Nd OIB array plotting among the field defined by Lana'i shield tholeiites [*Abouchami et al.*, 2005; *Gaffney et al.*, 2005] (Figure 8b).

[16] The alkalic lavas have high $^{143}Nd/^{144}Nd$ (0.51306–0.51308) and $^{176}Hf/^{177}Hf$ (0.28315–0.28317) and low $^{87}Sr/^{86}Sr$ (0.70305–0.70328) isotopic ratios, similar to rejuvenated lavas from Kaua'i and O'ahu (Table 3 and Figure 8). The alkalic lavas have low $^{208}Pb/^{204}Pb$ compared to tholeiitic basalts with similar $^{206}Pb/^{204}Pb$ (Figure 9).

6. Discussion

6.1. Volcanism West of Ka'ena Ridge

[17] The clusters of submarine volcanic cones west of Ka'ena Ridge are products of a low-volume tholeiitic phase of volcanism that occurred between Kaua'i and O'ahu circa 4.9 to 3.6 Ma. The timing of this volcanism overlaps and falls between tholeiitic shield-building volcanism on Kaua'i (5.1–4.0 Ma) and Wai'anae Volcano (3.9–3.1 Ma). The closest shield-like feature to these volcanic cones is a low-relief shield (20–35 km east) on the western end of Ka'ena Ridge that rises ~200 m above the surrounding submerged platform (Figures 1 and 2). West Ka'ena cones may be the products of distal eruptions from this volcanic edifice. The volcanism west of Ka'ena Ridge is an uncommon type of tholeiitic volcanism in the Hawaiian Islands in that it formed astride the main axis of the Hawaiian chain but was not associated with a large subaerial shield volcano (i.e., near a rift zone or the submarine flank of a subaerial shield volcano). The submarine cones retain their primary morphology and in this study volcano volume of the Hawaiian Islands is estimated along axis of the Hawaiian Chain rather than by age.

[18] Submarine volcanism west of Ka'ena Ridge represents a period of minimal magma production in the Hawaiian Islands, in terms of volcano volume per area, and therefore is an important reference point for sampling the evolution of the Hawaiian plume. New geochemical data of lavas collected from these cones reveal they consist primarily of tholeiitic and transitional basalts with major and trace element compositions that overlap those of shield stage basalts along the Hawaiian chain. Although the West Ka'ena tholeiitic cones are very small in volume compared to adjacent Hawaiian shield volcanoes, the lavas span a considerable range of the shield stage compositions and define a group of tholeiitic basalts with distinct trace element ratios (Sr/Nb, La/Nb) and Pb isotopic compositions. Trace element melting models indicate a moderately high degree of melting (8%–15%) comparable to Hawaiian shield volcanoes despite the low productivity of volcanism (Figure 7a).

[19] The flat-topped and conical submarine cones west of Ka'ena Ridge formed isolated volcanic centers through steady centralized effusive eruptions. These cones probably formed as overflowing submarine lava ponds from a levee surrounding a seafloor vent [*Clague et al.*, 2000]. The formation of submarine volcanic cones of similar size and shape is attributed to effusive eruption of lava with low volatile contents, high hydrostatic pressure at moderate to great ocean depth, long-lived steady eruption (years to decades), moderate effusion rates (assuming 0.1 km^3/year), and eruption on low-degree slopes [*Clague et al.*, 2000].

[20] All indicators (geology, geochronology, major and trace element, and isotopic compositions) show that the alkalic lavas, which mostly erupted as part of young lava fields sampled during Dive 296, are similar to the rejuvenated Kōloa Volcanics from Kaua'i [*Garcia et al.*, 2010]. Their young ages (1.39–0.24 Ma) confirm that these alkalic lavas are a form of late stage volcanism that was secondary to the main tholeiitic phase. Contrasting with onshore rejuvenated lavas, such as the Kōloa Volcanics, this form of secondary volcanism was well offshore and could be analogous to the submarine volcanic field west of Ni`ihau [*Clague et al.*, 2000] and other rejuvenated stage lavas that occur offshore of Hawaiian shield volcanoes [*Clague et al.*, 2003]. The alkalic basalts have major elements and trace element ratios similar to Kaua'i rejuvenated lavas, which were modeled to result from deep (3.5–4.0 GPa) very low degree (0.02%–2.6%) partial melting of a peridotite source [*Garcia et al.*, 2010]. The tholeiitic, transitional, and alkalic lavas from west of Ka'ena Ridge together provide an opportunity to examine volcanism spanning greater than 4.5 Myr along a section of the Hawaiian chain between subaerial shield volcanoes.

[21] The goals of sections 6.2–6.4 are to evaluate (1) source composition for West Ka'ena tholeiitic and transitional lavas compared to Hawaiian shield tholeiites, (2) pyroxenite versus peridotite source lithology for West Ka'ena lavas, and (3) the relationship between source composition and lithology to volume flux in the Hawaiian Islands.

6.2. Source Composition for Tholeiitic and Transitional West Ka'ena Lavas Compared to Hawaiian Shield Lavas

[22] The tholeiitic and transitional basalts from West Ka'ena are distinct in combined Pb-Sr-Nd-Hf isotopic systems from any lavas sampled in the Hawaiian Islands. Isotopic compositions of West Ka'ena lavas extend to extremely low $^{206}Pb/^{204}Pb$ and to a lower $^{208}Pb/^{204}Pb$ ratio than any Hawaiian tholeiitic lava (Figure 9). Several West Ka'ena samples have similar $^{206}Pb/^{204}Pb$ to SiO_2-enriched lavas of Ko'olau Makapu'u, Lāna'i, and Kaho'olawe [e.g., *Frey et al.*, 1994; *Huang et al.*, 2005]. However, compared to these lavas, the West Ka'ena lavas have higher Hf and Nd and lower Sr isotopic compositions but do not have elevated $^{208}Pb/^{204}Pb$ ratios at a given $^{206}Pb/^{204}Pb$ (Figure 9). West Ka'ena lavas have a high degree of variability in Pb isotope compositions compared to most Hawaiian shields, and their low volume and eruption from isolated cones may be an important factor. The relatively wide range in $^{208}Pb/^{204}Pb$ of West Ka'ena lavas is unmatched by any Hawaiian shield volcano.

[23] Large-scale intershield isotopic heterogeneity in the Hawaiian Islands has been defined by the distinction between the southern Loa trend and northern Kea trend volcanoes [*Tatsumoto*, 1978] (Figure 1). The spatial distribution of this large-scale bilateral asymmetry of Hawaiian shield volcanoes has been explained by (1) a concentrically zoned model [e.g., *Lassiter et al.*, 1996], (2) radially zoned plume model [*Bryce et al.*, 2005], (3) a bilaterally zoned plume model [*Tatsumoto*, 1978; *Abouchami et al.*, 2005], (4) a partly ordered zonation model [*Herzberg*, 2005], (5) a randomly distributed heterogeneity model [*Frey and Rhodes*, 1993; *Huang and Frey*, 2005; *Ren et al.*, 2006], and (6) vertically stacked heterogeneities [*Blichert-Toft et al.*, 2003]. The Loa trend is defined by

lower Pb, Nd, and Hf and higher Sr isotopic ratios, whereas lavas of the Kea trend typically have higher Pb, Nd, and Hf and lower Sr isotopic ratios [*Abouchami et al.*, 2005] (Figures 8 and 9). Loa-type lavas have been recognized among the southern volcanoes between Mauna Loa and Ko'olau, and Kea-type lavas are common among the northern subchain of volcanoes between Kīlauea and Kaua'i, as well as throughout the Hawaiian-Emperor chain [*Tanaka et al.*, 2008]. West Ka'ena lavas have similar Sr, Nd, and Hf isotopic compositions to lavas from Loa trend volcanoes but a group of lavas have lower $^{208}Pb/^{204}Pb$ and $^{206}Pb/^{204}Pb$ (Figure 9). Thus, our results demonstrate that Loa-type magmatism extends beyond Ko'olau volcano to circa 4.9 Ma and that it occurred prior to the development of the dual chain of volcanoes.

[24] The source of the Loa and Kea geochemical lines are thought to consist of small-scale heterogeneities [e.g., *Frey and Rhodes*, 1993; *Rhodes and Hart*, 1995; *Marske et al.*, 2007, 2008]. Isotope variation of Hawaiian basalts is usually attributed to melting of different proportions of heterogeneities of recycled material in the plume [e.g., *Ren et al.*, 2009]. West Ka'ena lavas may be influenced by these local-scale heterogeneities. Many of the West Ka'ena tholeiitic and transitional lavas have compositions that are displaced from the main Hawaiian shield array, similar to postshield lavas from Hualālai volcano [*Hanano et al.*, 2010]. The samples with the least radiogenic Pb compositions deviate from the main shield array toward less radiogenic Sr and Pb isotopic compositions, and more radiogenic Nd. These deviations indicate that the West Ka'ena tholeiitic lavas cannot be explained by mixing of the Ko'olau and Kea end-members [e.g., *Blichert-Toft et al.*, 1999]. Instead, the group of West Ka'ena lavas with low Pb isotope compositions sampled a distinct component that is not regularly sampled by Hawaiian shield lavas or define an isolated compositional heterogeneity. However, the group of West Ka'ena lavas with higher Pb isotopes overlap the main field of Loa volcanism (Figure 9). The low Pb component cannot be Pacific oceanic crust because the Pb isotopic composition of Pacific crust is too radiogenic and Pb-Pb mixing lines do not intersect Pacific MORB compositions (Figure 9). This combination of evidence suggests that the lavas west of Ka'ena Ridge formed from recycled material within the Hawaiian plume and these extreme Pb isotope compositions may be present in distinct heterogeneities or sampled preferentially under specific melting conditions or area of the plume.

[25] Trace element ratios combined with isotope compositions provide insights on the nature of heterogeneities (lithologic versus isotopic heterogeneities, type of recycled material). West Ka'ena lavas, compared to Hawaiian shield lavas, highlight the differences between Loa and Kea trend lavas (Figure 10). Sr/Nb and La/Nb of West Ka'ena lavas correlate with $^{206}Pb/^{204}Pb$ and West Ka'ena volcanics are the only individual suite of lavas that form a clear trend in these plots. The tholeiitic basalts from Hawaiian shields as a whole form a broad overall trend in these trace element ratios and Pb and Sr isotope ratios (Figure 10). Compared to Kea-type lavas, Loa-type volcanism generally has lower Pb and higher Sr isotope ratios, higher Sr/Nb and La/Nb, and lower Th/La than Kea-type lavas. West Ka'ena samples exemplify these characteristics. The correlation of trace element ratios and Pb isotope ratios in West Ka'ena lavas indicates this relationship is related to the composition of the source and is not solely controlled by partial melting effects or degree of crystal fractionation. Correlation of trace element and isotope ratios between Hawaiian shields reflects tapping of multiple, distinct source components or differences in the proportion of source components [*Frey and Rhodes*, 1993]. Variation of Sr/Nb and La/Nb and isotopes in Hawaiian lavas has been attributed to (1) melting of garnet pyroxenite that originated from a recycled plagioclase-rich gabbroic component and (2) a small sedimentary component derived from ancient phosphate-bearing carbonate [*Huang and Frey*, 2005]. *Huang and Frey* [2005] suggested that high Sr/Nb and La/Nb, and low Th/La in Ko'olau lavas are characteristic of enrichment in marine sediments, which also typically possess lower $^{238}U/^{204}Pb$ than primitive mantle which would lead to low $^{206}Pb/^{204}Pb$ ratios. Low Th/La ratios, negative Th-U anomalies, and positive Sr anomalies have been identified with a recycled gabbroic component based on the partitioning of these elements in plagioclase in oceanic crust [*Hofmann and Jochum*, 1996; *Sobolev et al.*, 2000]. The correlation between intershield differences in some incompatible element ratios (e.g., Sr/Nb, La/Nb) and isotope ratios, indicates that each shield has been formed from a *compositionally* distinct source with small-scale heterogeneities [*Putirka*, 1999].

[26] Several lines of evidence preclude a significant role for recycled marine sediments in the source of West Ka'ena lavas, assuming the composition of

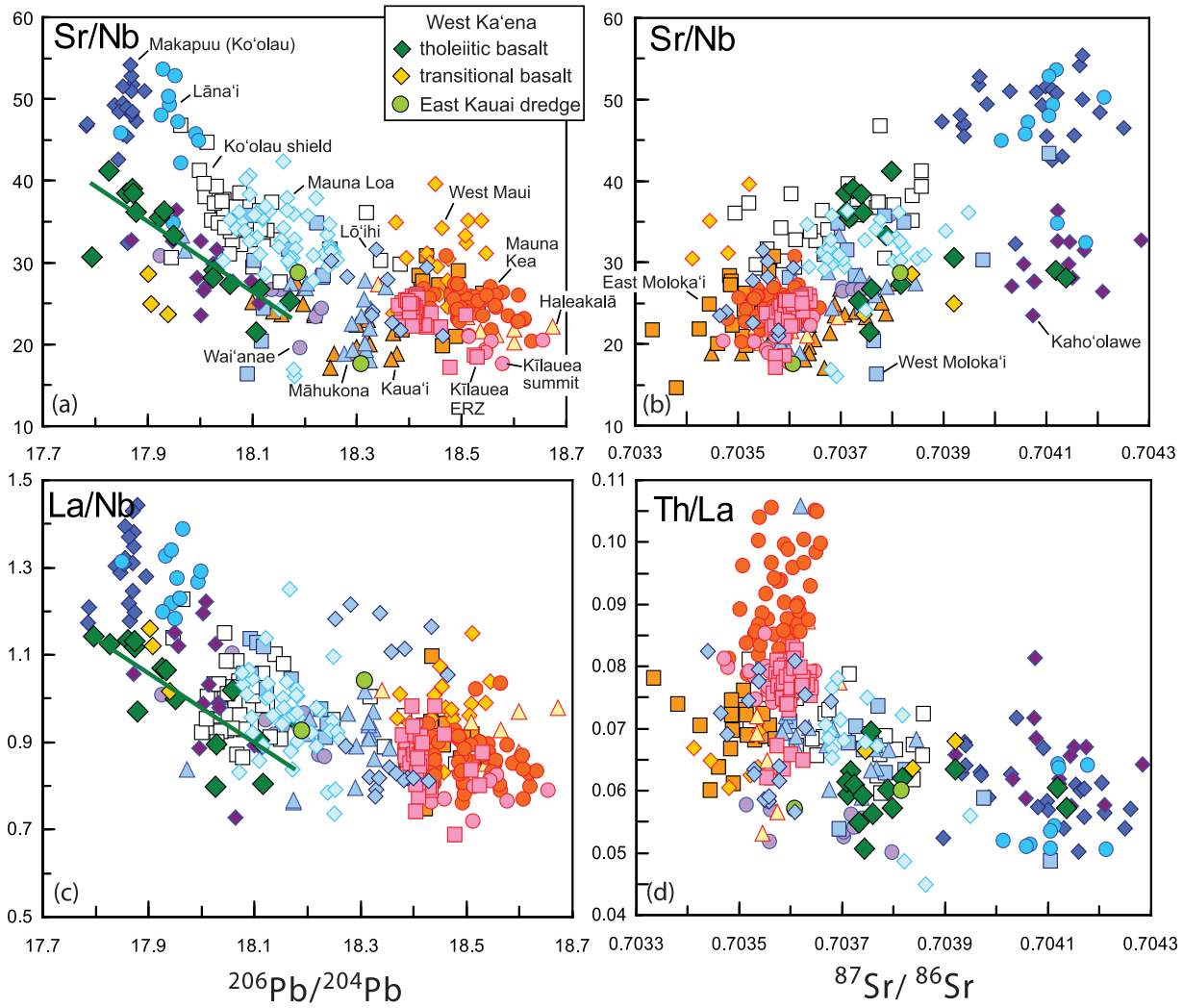

Figure 10. Trace element ratios versus Pb and Sr isotope compositions for Hawaiian shield volcanoes. (a) Sr/Nb versus $^{206}Pb/^{204}Pb$. (b) Sr/Nb versus $^{87}Sr/^{86}Sr$. (c) La/Nb versus $^{206}Pb/^{204}Pb$. (d) Th/La versus $^{87}Sr/^{86}Sr$. References for data sources are listed in the auxiliary material (Text S1). Green line is a best fit line for West Ka'ena tholeiitic basalts. Symbols for each Hawaiian shield volcano are labeled in Figures 10a and 10b. Symbols for Loa trend volcanoes are in cooler (bluish) colors, and Kea trend volcanoes are in hotter (reddish) colors. All isotope data from Hawaiian shield volcanoes are normalized to the same set of standards. Alkalic lavas from west of Ka'ena Ridge and other rejuvenated lavas are not shown in these plots.

sediments has not been significantly modified during recycling. A sedimentary component with high Rb/Sr would lead to high Sr isotope ratios and a positive correlation between Rb/Sr and $^{87}Sr/^{86}Sr$, as suggested by *Huang et al.* [2009] for Mahukona lavas; there is no correlation between Rb/Sr and $^{87}Sr/^{86}Sr$ in West Ka'ena lavas. A positive correlation is apparent between Zr/Nb and Sr/Nb (not shown), which is not expected from a recycled carbonate, sediment source. Marine sediments usually have higher $^{232}Th/^{238}U$ and lower $^{238}U/^{204}Pb$ than primitive mantle and therefore recycled sedimentary material is characterized by high $^{208}Pb/^{204}Pb$ relative to $^{206}Pb/^{204}Pb$; West Ka'ena lavas do not have high $^{208}Pb/^{204}Pb$ relative to $^{206}Pb/^{204}Pb$ as observed in Ko'olau lavas. Radiogenic ingrowth of sediments with high Lu/Hf leads to high $^{176}Hf/^{177}Hf$ relative to $^{143}Nd/^{144}Nd$; this relationship is not evident in West Ka'ena lavas (with the exception of the one sample, 305-04). High $^{176}Hf/^{177}Hf$ for this sample may reflect greater contribution from a depleted lithosphere component [*Salters et al.*, 2006]. There is also no apparent correlation between Ce/Pb and La/Nb or Th/La, which is anticipated by low-Ce/Pb sediments (although Ce/Pb of whole rocks may be

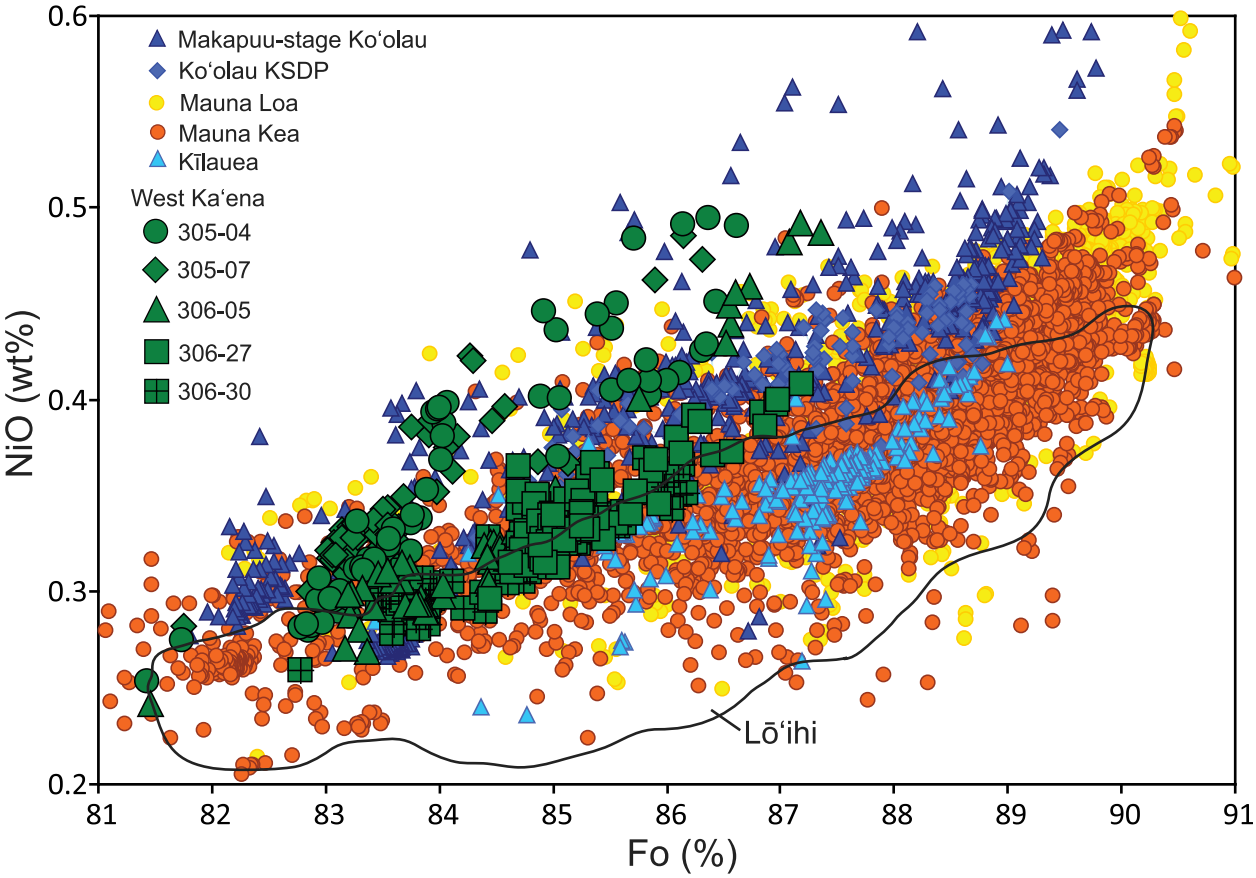

Figure 11. NiO (wt %) versus Fo content (%) for olivines from West Ka'ena lavas compared to olivines from tholeiitic basalts from several Hawaiian shield volcanoes (Ko'olau, Mauna Loa, Mauna Kea, and Lō'ihi). Olivine compositions from Hawaiian shield volcanoes are from *Sobolev et al.* [2007].

affected by alteration [*Hofmann*, 2003; *Huang and Frey*, 2005]). West Ka'ena lavas have Loa-type trace element and isotopic compositions that are distinct from the extreme Loa-type lavas from Makapu'u stage Ko'olau and Lāna'i (e.g., they lack comparably high Sr/Nb, La/Nb, and $^{87}Sr/^{86}Sr$) that has been attributed to a recycled sedimentary component.

6.3. Pyroxenite Versus Peridotite Source for West Ka'ena Lavas

[27] Several key geochemical and seismological observations support that the Hawaiian hot spot originates as a deep-seated, high-temperature plume from the lower mantle [e.g., *DePaolo and Manga*, 2003; *Montelli et al.*, 2004; *Wolfe et al.*, 2009]. Geochemistry of Hawaiian shield lavas suggests the Hawaiian plume consists partly of recycled oceanic crust [*Blichert-Toft et al.*, 1999; *Gaffney et al.*, 2005; *Hauri*, 1996; *Herzberg*, 2006; *Lassiter and Hauri*, 1998; *Sobolev et al.*, 2000, 2005, 2007]. Oxygen isotopes of olivines from Hawaiian shield lavas also indicate a component of hydrothermally altered rocks, perhaps derived from Cretaceous oceanic crust beneath Hawai'i or earlier erupted Hawaiian lavas, in the source of Hawaiian shield basalts [e.g., *Eiler et al.*, 1996]. One of the fundamental questions from geochemistry is the importance and nature of mafic lithologies in the mantle source of Hawaiian basalts.

[28] The Hawaiian plume is thought to consist of a peridotite matrix with finely distributed streaks or parcels of recycled eclogite or pyroxenite, perhaps superimposed on the larger-scale, plume-wide Loa-Kea asymmetry [e.g., *Kogiso et al.*, 2004; *Reiners*, 2002; *Ren et al.*, 2009]. Pyroxenite and peridotite undergo different degrees of partial melting and these melts may react with surrounding plume material and mix in at shallower levels during ascent [*Pertermann and Hirschmann*, 2003; *Reiners*, 2002; *Sobolev et al.*, 2005]. The emergence of different proportions of pyroxenite- and

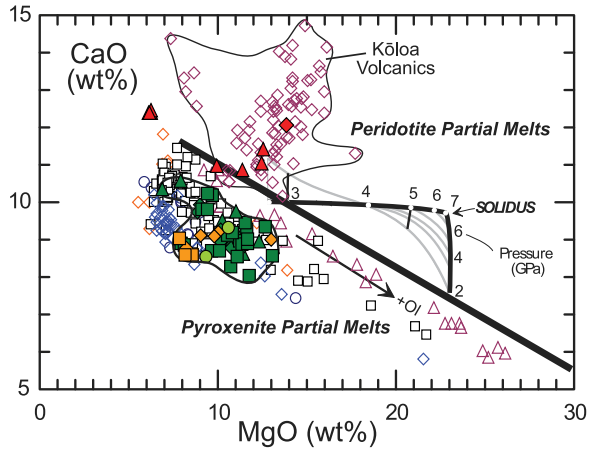

Figure 12. CaO versus MgO of West Ka'ena lavas compared to lavas from Hawaiian shield volcanoes. Symbols are the same as in Figures 8 and 9. Lavas with CaO contents lower than the black line are potential pyroxenite partial melts, and compositions above the black line are similar to lavas that form from peridotite source melts [*Herzberg and Asimow*, 2008].

peridotite-derived melts may be controlled by the thermal structure of the plume and spatial distribution of lithologic heterogeneities [*Ren et al.*, 2009], which may be a function of proximity to the central axis of the plume, plume flux, and/or plate thickness or motion [*Sobolev et al.*, 2007; *Vidal and Bonneville*, 2004; *White*, 1993].

[29] A pyroxenite source model for Hawaiian tholeiites contends that the Ni concentrations of olivines in these lavas should be a reflection of the Ni concentration and the presence of olivine in the source [*Sobolev et al.*, 2005, 2007]. Therefore, olivines crystallizing in melts derived from Ni-rich peridotite should be lower in NiO (as a result of the high compatibility of Ni in olivine). Melts from a pyroxenite source and their crystallizing olivines should be enriched in NiO, because olivine is not controlling the partitioning of Ni. *Sobolev et al.* [2005] demonstrated that olivines and calculated parental magmas of *some* shield stage Hawaiian tholeiites have high Ni contents compared to other oceanic islands, MORB, and Gorgona komatiites. They proposed a model of melting of eclogite and reaction of this melt with peridotite to produce an olivine-free pyroxenite source for Hawaiian magmas, which dictates excess NiO in some lavas. Lavas erupted on Ko'olau and Mauna Loa volcanoes have olivines with the highest NiO at a given Fo content and are proposed to involve the greatest contribution of pyroxenite-derived melt [*Sobolev et al.*, 2005]. This interpretation is consistent with the presence of high-SiO_2 lavas in these and other Loa-type volcanoes, which is expected for melting of a recycled eclogite [*Kogiso et al.*, 2003]. Ni contents in olivine in primitive (11–13 wt % MgO) West Ka'ena lavas provides a test for evaluating the contribution of pyroxenite-derived melts, based on the method of *Sobolev et al.* [2005].

[30] Olivine phenocrysts in five West Ka'ena tholeiitic lavas were analyzed using analytical conditions similar to the ones used by *Sobolev et al.* [2005] (the results are compared to the large database of olivine compositions from Hawaiian shield basalts presented by *Sobolev et al.* [2007] (Figure 11; see Appendix A for summary of analytical methods)). Olivine phenocrysts form two broad bands in NiO (wt %) versus Fo (%). Olivines from three West Ka'ena lavas (305-04, 305-07, 306-05) have similar NiO to Ko'olau lavas at a given Fo content, whereas olivines from two samples overlie compositions of olivines for the main field of Hawaiian shield basalts from Mauna Loa, Mauna Kea, and early/middle Ko'olau. Sample 305-04 is of particular interest because it has olivines with the highest NiO, and whole-rock composition with the lowest $^{206}Pb/^{204}Pb$ and high SiO_2 (51.7 wt %) [this sample has multiple olivine populations suggesting it picked up olivine, probably from the cumulate pile, as found on other Hawaiian volcanoes (Kīlauea [*Clague et al.*, 1995]; Mauna Loa [*Garcia et al.*, 1995]; and Ko'olau [*Garcia*, 2002]). These are characteristics similar to the Ko'olau Makapu'u stage (late stage) lavas, proposed to have a significant contribution of pyroxenite-derived melt [*Hauri*, 1996; *Sobolev et al.*, 2005]. Interestingly, sample 305-04 is also the only West Ka'ena sample that lies well above the Hawaiian Hf-Nd isotope array (Figure 8), indicating contribution from a depleted lithosphere component [*Salters et al.*, 2006] or marine sedimentary component [*Blichert-Toft et al.*, 1999]. Whole-rock trace element and isotope compositions do not support contribution from recycled marine sediments (see previous discussion). Sample 306-05 has olivines that fall on both trends. Based on the high Ni contents (and high Fe/Mn and low CaO) of some olivines in West Ka'ena lavas, in combination with the whole-rock trace element and isotope compositions compared to Hawaiian shield basalts, West Ka'ena lavas likely involved contribution from melting of pyroxenite.

[31] Another origin for high-Ni olivines has been proposed *Wang and Gaetani* [2008] based on experimental data on partitioning of Ni between olivine and siliceous eclogite partial melts. *Wang and Gaetani* [2008] suggested that Ni is more

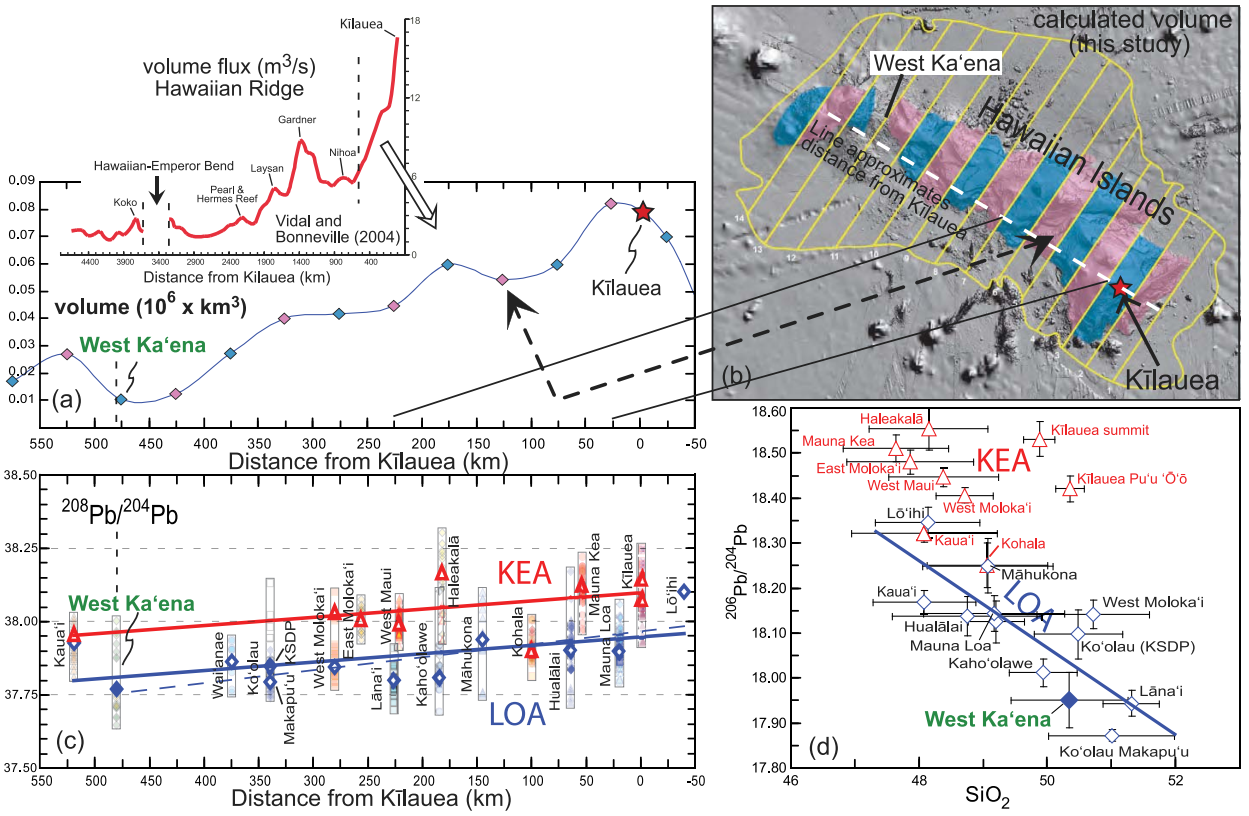

Figure 13. Estimated volume of the Hawaiian Islands compared to Pb isotope compositions and SiO_2 of Hawaiian shield stage basalts. (a) Volume ($10^6 \times km^3$) at the center of a series of 50 km wide bins shown in Figure 13b versus distance from Kīlauea (km). Inset shows volume flux (m^3/s) for the Hawaiian Ridge from *Vidal and Bonneville* [2004], with dashed line at 550 km indicating the start of volume calculations in this study. (b) Map of the Hawaiian Islands showing area used for volume calculations and 50 km wide bins approximately perpendicular to the axis of the islands. Volume estimates for pink and blue colored bins are indicated by pink and blue symbols in Figure 13a, plotted at a distance from Kīlauea at the right edge of the bin, where the small white numbers are for the bin. (c) Plot of $^{208}Pb/^{204}Pb$ versus distance from Kīlauea (km) with averages shown for individual shields. Linear regressions are shown for Kea (red) and Loa (blue) trend volcanoes. Dashed blue regression line does not include Kaua'i. (d) Average $^{206}Pb/^{204}Pb$ versus SiO_2 for individual shield volcanoes. Bars represent one standard deviation. Most of the lavas in this compilation have been filtered for alteration (e.g., $K_2O/P_2O_5 > 1$). References for data sources for isotope and major element data are listed in the auxiliary material (Text S1). All isotope data from Hawaiian shield volcanoes are normalized to the same set of standards. Alkalic lavas from west of Ka'ena Ridge and other rejuvenated lavas are not shown in these plots. Kaua'i and West Moloka'i are divided into Loa and Kea compositions in Figures 13c and 13d based on *Garcia et al.* [2010] and *Xu et al.* [2007], respectively. Volcano volume is calculated by assuming the base of the volcano is the surface of the preexisting Pacific seafloor. This surface was determined by first extrapolating the surface of the seismically determined, base of the preexisting oceanic crust (i.e., Moho) [*Watts and ten Brink*, 1989] and then shifting it upward by 6 km, to account for the assumed uniform crustal thickness. We then calculated the volume between the top of the preexisting Pacific seafloor and the high-resolution bathymetry and subaerial topography (see *Robinson and Eakins* [2006] for bathymetry and topography data sources and further details of volume calculations). The volume of the compacted moat sediments was computed by multiplying their assumed average thickness of 500 m by the area of the edifices; this volume was then subtracted from the total. Volumes are minimum estimates because they also ignore the large debris avalanches deposited on the archipelagic aprons. Volume calculations are shown in 50 km bins perpendicular to the axis of the islands, rather than by volcano, because of the difficulty in delineating the boundary of each volcano below the surface [see *Robinson and Eakins*, 2006]. Subsidence, landsliding, sedimentation, and intrusion between Kaua'i and O'ahu will not significantly effect volume calculations for West Ka'ena or obscure the increasing volume along the Hawaiian Islands.

compatible in olivine crystallizing from siliceous melts than in basaltic melts, and that Hawaiian lavas with high Ni (e.g., Ko'olau Makapu'u stage lavas) may have formed from mixing of reacted high-SiO_2 eclogite partial melt with primitive basalt. However, based on careful evaluation of partition coefficients and Fe/Mn ratios from *Wang and Gaetani* [2008], *Gurenko et al.* [2009] concluded that the experimental data failed to explain Fe/Mn ratios. Thus, *Gurenko et al.* [2009] suggested variations of Ni in olivines from Canary Island shield lavas are likely due to varying pyroxenite/peridotite in the source rather than from mixing and crystallization of SiO_2-rich melts as suggested by *Wang and Gaetani* [2008]. Using the equations of *Gurenko et al.* [2009], the proportion of pyroxenite-derived melt relative to peridotite-derived melt in West Ka'ena lavas is estimated between 0.65 to 0.77.

[32] Major element compositions of lavas also help constrain source lithology. Hawaiian shield lavas have low CaO contents compared to model CaO contents of partial melts of peridotite and similar CaO to many experiments of pyroxenite melting (Figure 12) [*Herzberg and Asimow*, 2008]. Partial melts of pyroxenite have low CaO because of the strong influence of residual clinopyroxene in the source [*Herzberg*, 2006]. West Ka'ena lavas have similar whole-rock CaO contents to other shield stage lavas in Hawai'i (Figure 12). The low CaO of West Ka'ena lavas and Hawaiian shield lavas suggest a significant role for melting of pyroxenite in the Hawaiian plume. Whereas, the alkalic lavas from west of Ka'ena Ridge and rejuvenated lavas from the Hawaiian Islands have high CaO contents that are similar to melts derived from peridotite sources. West Ka'ena lavas are some of the earliest examples of Loa-type volcanism in the Hawaiian Islands (circa 4.9 Ma) that indicate melting of a pyroxenite source, and thus provide insights on the evolution of the Hawaiian Islands.

6.4. What Is the Relationship of Source Composition and Lithology to Volume Flux in the Hawaiian Islands?

[33] The Hawaiian-Emperor Chain is the longest example of an island chain on Earth, both in time and space, active for 80 Myr and extending almost 6000 km. One of the distinctive features of the Hawaiian-Emperor Chain is the dramatic and rapid variation in magma flux rate along the Hawaiian Ridge (<30 Ma), and particularly along the Hawaiian Islands. The activity of the Hawaiian hot spot has increased by ~300% in the last 30 Myr and this increase has been most dramatic over the last 3 Myr [*Vidal and Bonneville*, 2004] (Figure 13a, inset). An opposite trend of decreasing melt flux with age is observed for the Louisville chain [*Lonsdale*, 1988] and Walvis and St. Helena hot spots [*Adam et al.*, 2007]. It has been suggested that the Loa component only recently emerged in the Hawaiian chain (<3 Ma) [*Abouchami et al.*, 2005] and is related to a pyroxenite source [*Hauri*, 1996], which in most cases melts at a lower temperature and to higher extent than peridotite [*Stracke and Bourdon*, 2009]. These observations were combined to suggest that the recent appearance of pyroxenite is the cause of the large magma flux for the Hawaiian Islands [*Tanaka et al.*, 2008]. However, our new data indicate the presence of Loa-type isotopic characteristics in low-volume, >3 Myr old lavas from West Ka'ena and melting of pyroxenitic source material (Figures 13c and 13d).

[34] Determining the relationship between mantle source composition, lithology and volume flux in the Hawaiian Islands can impact our thinking about the evolution of the Hawaiian hot spot and provides constraints on the mechanisms of large-scale melt flux variations [*White*, 1993]. Proposed mechanisms to account for melt flux variations involve shallow (lithosphere) or deep (plume) processes. Lithosphere-related explanations include (1) plate thickness variations or lithospheric features (e.g., fracture zones) [*Hieronymus and Bercovici*, 1999; *Regelous et al.*, 2003; *White*, 1993] and (2) changes in plate stresses resulting from reconfigurations of plate motion [*Wessel and Kroenke*, 2009]. Plume-related causes include (1) southward migration of the Hawaiian hot spot [*Tarduno et al.*, 2003; *Wright and Klein*, 2006], (2) periodic oscillation in the plume conduit [e.g., *Ito*, 2001; *Sleep*, 1992; *van Keken and Gable*, 1995], and (3) changes in source composition and/or melting conditions [*Lee et al.*, 2009; *Sobolev et al.*, 2007]. Here we evaluate changes in source composition and volume flux in the Hawaiian Islands.

[35] Hawaiian shield volcanoes show dramatic changes in their source composition [*Tatsumoto*, 1978; *Stille et al.*, 1983; *Staudigel et al.*, 1984; *Abouchami et al.*, 2005]. Our new volume calculations for the Hawaiian Islands reveal a dramatic increase in magma production rate since circa 4.5–4.0 Ma (Figures 13a and 13b; the new volume calculations are described in the caption of Figure 13). The excellent geochemical coverage for the Hawaiian Islands, along with the new isotopic analyses between Kaua'i and O'ahu, has allowed

us to identify a correlation between Pb isotopic composition, major element composition, and volume flux in the Hawaiian Islands. Average $^{208}Pb/^{204}Pb$ ratios for Hawaiian shield volcanoes show a resolvable systematic increase with decreasing age (or distance from Kīlauea) for both Kea and Loa trend volcanoes (Figure 13c). West Ka'ena lavas have the lowest average $^{208}Pb/^{204}Pb$ and form the lowest volume along the axis of the Hawaiian Islands. Both volume and $^{208}Pb/^{204}Pb$ increase from a local minimum near West Ka'ena toward a peak centered on Mauna Loa and flanked by Mauna Kea and Kīlauea. Although trends in $^{208}Pb/^{204}Pb$ versus age are observed within the Loa and Kea volcano trends individually, Loa trend volcanoes have systematically lower $^{206}Pb/^{204}Pb$ ratios than Kea trend volcanoes. Average $^{206}Pb/^{204}Pb$ correlates with SiO_2 for Loa trend volcanoes (Figure 13d). Kea trend volcanoes do not show this systematic variation between Pb isotopes and SiO_2. The variation in Pb isotopes in the Loa trend volcanoes is also about 1.5 times that of the Kea trend volcanoes. There is no correlation between the individual volcano volumes, from *Robinson and Eakins* [2006], and average $^{206}Pb/^{204}Pb$ or SiO_2 for individual volcanoes (not shown).

[36] There are several possible explanations for the correlation between increasing volume flux and major element and isotopic composition in Hawaiian lavas: (1) increasing pyroxenite in the source, (2) changing composition of pyroxenite in the source, (3) increasing temperature of the plume, (4) increasing plume flux (i.e., material supplied by the plume), (5) migration or tilting of the plume, and (6) change in plate motion. Our results provide constraints on pyroxenite in the source based on lava composition and volcano volumes along the Hawaiian chain. If the low Pb isotopic ratios are representative of the pyroxenite source of Hawaiian lavas (West Ka'ena, Ko'olau Makapu'u, Lāna'i, Kaho'olawe) and pyroxenite is more fusible than the higher $^{208}Pb/^{204}Pb$-$^{206}Pb/^{204}Pb$ peridotite source material, then in the simplest case, an increasing volcano volume should correlate with decreasing, not increasing Pb isotope ratios toward Kīlauea. Therefore, if the increase in volcano volume is related to an increase in pyroxenite content in the source, the observed compositional trend would require the radiogenic Pb content of the pyroxenite source to change with time. The positive relationship between radiogenic Pb and volcano volume suggests an additional factor besides the proportion of pyroxenite in the source is changing with time. Another possible interpretation is that the temperature of plume or plume flux has been increasing and the amount of pyroxenite in the source has not significantly increased. However, our study does not provide constraints on mantle temperature or plate motion, so we cannot evaluate these possibilities.

[37] The Hawaiian Islands are rare among ocean island basalts in that they display evidence for a silica-rich pyroxenite source, perhaps from melting beneath relatively thick lithosphere (~100 km thick beneath the Big Island [*Li et al.*, 2004]) compared to Iceland and Galāpagos [*Jackson and Dasgupta*, 2008; *Sobolev et al.*, 2007]. Our new data and previous work [e.g., *Hauri*, 1996] suggest pyroxenite (recycled oceanic crust) sampled at different phases of the Hawaiian plume (e.g., West Ka'ena, Ko'olau) has low time-integrated U/Pb ratios. This is not always the case for recycled oceanic crust (e.g., HIMU in the Canary Islands) [*Jackson and Dasgupta*, 2008; *Gurenko et al.*, 2009]. Loa-type magmatism, commonly attributed to mafic lithologies in the source [*Hauri*, 1996], occurs at times of the highest (Mauna Loa) and lowest (West Ka'ena) productivity in the Hawaiian Islands. This also suggests the increasing volume of the Hawaiian Islands may not be controlled primarily by the amount of entrained mafic lithologies in the Hawaiian plume. The appearance of Loa-type volcanism may not be independently related to increase in volume flux. The emergence of greater proportions of the pyroxenite component in Loa-type magmatism has been proposed to be related to the thermal structure of the Hawaiian plume, distribution of heterogeneities, and the solidus temperature of pyroxenite heterogeneities [*Reiners*, 2002; *Ren et al.*, 2009]. Initiation of pyroxenite melting can be considerably deeper than peridotite (depending on the composition of the pyroxenite) and preservation and abundance of pyroxenite-derived melt depends on (1) extent of pyroxenite melting prior to peridotite melting, (2) relative masses of pyroxenite and peridotite, and (3) how pyroxenite and peridotite melts mix and interact with surrounding mantle during ascent [*Stracke and Bourdon*, 2009]. Pyroxenite melts may become increasingly diluted as the extent of peridotite melting increases and therefore melts extracted from greater depth may contain greater proportion of pyroxenite-derived melt (assuming melts do not react at high pressure to precipitate pyroxenite) [*Kogiso et al.*, 2004; *Herzberg and Asimow*, 2008]. For lavas west of Ka'ena Ridge, melts may have formed along the margin of the

central axis of the plume and perhaps avoided substantial mixing with melts from shallower peridotite sources. This is due to less upwelling away from the center of the plume axis, as plume material is transported laterally [e.g., *Ribe and Christensen*, 1999]. This may have lead to a melting column with a deep zone of largely melted pyroxenite and a restricted amount of small-degree peridotite melt from shallower levels [*Reiners*, 2002]. Another possibility is these melts may have formed later than the main phase of volcanism that created the low shields on Ka'ena Ridge and the melts may have been extracted from increasing depths, which increased the proportion of pyroxenite melts and decreased contribution from peridotite melting. Also, the nature of the eruptions that formed the submarine cones west of Ka'ena Ridge, at isolated volcanic centers through short-lived effusive eruptions (similar to rejuvenated volcanism), may have decreased the degree of mixing and homogenization between shallow and deeper melts in a centralized magma reservoir system.

[38] Lithospheric thickness and location of fracture zones may play a role in controlling the spacing of the volcanoes and the formation of parallel chains (Loa-Kea trends) [e.g., *Hieronymus and Bercovici*, 1999]. However, they do not appear to be responsible for the dramatic volume variation along the Hawaiian Islands. There is no correlation between magma production rate and lithosphere thickness or fracture zones [*White*, 1993; *Van Ark and Lin*, 2004; *Vidal and Bonneville*, 2004]. Periodic oscillation in the plume conduit [e.g., *Ito*, 2001] may cause perturbations in magma flux, but evaluation of a greater part of the Hawaiian chain is necessary to assess the role of solitary waves. Changes in Pacific plate motion due to plate boundary interactions affect the horizontal stresses in the lithosphere [e.g., *Sager and Keating*, 1984; *Koppers and Staudigel*, 2004; *Wessel and Kroenke*, 2007]. Depending on the direction of these changes and the location on the plate, a region may experience an increase in tensional or compressional stresses; these stresses may modulate the amount of melt that reaches the surface [*Hieronymus and Bercovici*, 1999].

7. Conclusions

[39] A field of tholeiitic submarine cones west of Ka'ena Ridge formed astride the axis of the Hawaiian Islands between 4.9 to 3.6 Ma. Their eruptions were contemporaneous with shield-building volcanism on the island of Kaua'i and Wai'anae Volcano on O'ahu. The longest distance between large subaerial shields of the Hawaiian Islands is between the islands of Kaua'i and O'ahu, where the volume of the islands is also the smallest. These cones sampled volcanism across the axis of the Hawaiian Islands (spanning ~70 km) during a time of minimal magma productivity and prior to formation of dual Loa and Kea geographical trends of volcanoes. The cones may be distal eruptions related to the low shields on Ka'ena Ridge. The lavas west of Ka'ena Ridge have distinct trace element and isotopic compositions compared to those of Hawaiian shield basalts, with the lowest Pb isotopic ratios in the Hawaiian Islands. Half of the volcanic cones contain high-SiO_2 basalts (51.0–53.5 wt % SiO_2), similar to Loa trend lavas of Ko'olau Makapu'u, Lāna'i, and Kaho'olawe. Samples with the lowest time-integrated U/Pb ratios reveal a contribution from pyroxenite-derived melts, based on olivines in several West Ka'ena lavas with high Ni contents compared to most Hawaiian shield basalts. The low Pb isotope compositions may have formed from pyroxenite under specific melting conditions, from local-scale heterogeneities, or possibly in the periphery of the plume without mixing with melts from shallower peridotite sources. Young lava fields (circa 0.37 Ma) sampled southwest of Ka'ena Ridge are related to secondary volcanism derived from a peridotite source.

[40] Tholeiitic volcanism west of Ka'ena Ridge provides insights about Loa-type volcanism and the evolution of the Hawaiian Islands.

1. Loa-type volcanism has persisted for at least 4.9 Myr along the Hawaiian Archipelago.

2. Volcanism between Kaua'i and O'ahu sampled Loa-type components without the complementary Kea component, prior to formation of a dual chain of volcanoes; this suggests vertical heterogeneity in the Hawaiian plume.

3. There is a resolvable correlation between volume flux and Pb isotope ratios in Hawaiian tholeiitic basalts, and a correlation between major elements and isotopes in Loa trend volcanism. The correlation between Pb isotope ratios and SiO_2 in the Loa trend volcanoes is evidence for variable influence of pyroxenite in these volcanoes. If the increase in volume flux in the Hawaiian Islands is due to increasing pyroxenite in the source, and unradiogenic Pb isotope ratios are representative of the pyroxenite source of Hawaiian lavas, then

increasing volcano volume should correlate with a trend of decreasing radiogenic Pb toward Kīlauea. It does not. Therefore, other factors besides the proportion of pyroxenite in the source are influencing the increase in volume flux (e.g., temperature, plume migration or oscillation in plume flux, or plate stresses).

4. The presence of Loa magmatism at times of the highest and lowest volume flux in the Hawaiian Islands suggests Loa-type volcanism may not be independently related to increase in volume flux or entrained mafic component in the Hawaiian plume (although further work along the older part of the Hawaiian Ridge (>6 Ma) is necessary to test this relationship).

Appendix A: Sample Preparation and Analytical Methods

A1. University of Wisconsin $^{40}Ar/^{39}Ar$ Dating Method

[41] The $^{40}Ar/^{39}Ar$ incremental heating experiments were undertaken on eleven West Ka'ena lava lavas. Holocrystalline groundmass separates were prepared from porphyritic lava samples by crushing, sieving to 250–350 μm, magnetic sorting, density separation using methylene iodide, and ultimately hand picking under a binocular microscope. Purified groundmass separates were weighed and then wrapped in 99.99% copper foil packets placed into Al disks with the 28.201 Ma Fish Canyon sanidine [*Kuiper et al.*, 2008], which monitors neutron fluence. The Al disks were irradiated for 3 h at the Oregon State University TRIGA reactor in the Cadmium-Lined In-Core Irradiation Tube (CLICIT) where they a received fast neutron dose of ~1.5×10^{15} n/cm^2. Based on previous experiments, corrections for undesirable nucleogenic reactions on ^{40}K and ^{40}Ca are: $[^{40}Ar/^{39}Ar]_K = 0.00086$; $[^{36}Ar/^{37}Ar]_{Ca} = 0.000264$; $[^{39}Ar/^{37}Ar]_{Ca} = 0.000673$. J values were uniform within analytical error across individual Al disks, and the precision of the J values averaged ±0.10% (2σ). The age uncertainty determined for each sample is the 2σ analytical error, unless otherwise noted.

[42] At the University of Wisconsin Rare Gas Geochronology Laboratory, ~20–25 mg of groundmass was placed in a 3 mm × 20 mm copper trough and incrementally heated using a 25 Watt CO_2 laser. Prior to each incremental heating experiment, samples were degassed at 2% power to potentially remove large amounts of water and atmospheric argon. Fully automated experiments consisted of 8–10 steps; each step included a scan across the trough at 150 μm/s at a given laser power, followed by an additional 15 min for gas cleanup. The gas was cleaned during and after the heating period with two SAES C50 getters. Argon isotope analyses were done using a MAP 215–50, and the isotope data was reduced using ArArCalc software version 2.4 [*Koppers*, 2002].

[43] Obtaining precise $^{40}Ar/^{39}Ar$ age determinations for Pleistocene volcanics requires careful characterization of blank levels in the analytical system and mass discrimination of the instrument. Blanks were measured after every two steps during the incremental heating experiment and interpolated. Mass discrimination was monitored daily via an automated air pipette and averaged 1.0000 ± 0.04% per atomic mass unit (a.m.u.) during the analytical period. Replicate experiments were performed on several samples to check for accuracy and improve precision. Isochron regressions [*York*, 1969] agree with plateau ages and do not reveal evidence that excess argon is present in any of the lavas, therefore, we consider the plateau ages to give the best estimate of the time elapsed since eruption (Table 1). All ages were calculated using the decay constants of *Steiger and Jäger* [1977]. For each analysis the uncertainties include estimates of the analytical precision on peak signals, the system blank, spectrometer mass discrimination, and reactor corrections. Criteria used to determine whether an incremental heating experiment gave meaningful results and to calculate plateau and isochron ages were (1) plateaus are defined by at least four contiguous steps all concordant in age at the 95% confidence level and comprising >50% of the ^{39}Ar released, (2) a well-defined isochron exists for the plateau points as defined by the F variate statistic SUMS/(N-2) [*York*, 1969], (3) the plateau and isochron ages are concordant at the 95% confidence level, and (4) the $^{40}Ar/^{36}Ar$ intercept for the isochron does not differ from the atmospheric value of 295.5 at the 95% confidence level.

A2. Kyoto University Unspiked K-Ar Dating

[44] Six of the freshest West Ka'ena lavas samples were selected for unspiked K-Ar dating, the preferred method for dating young samples with high atmospheric contamination [*Matsumoto et al.*, 1989]. K-Ar dating was done at Kyoto University

starting with 80–100 g of rock crushed in a stainless steel pestle. Samples were sieved to 180–250 μm, and washed with deionized water and then acetone in an ultrasonic bath. Phenocrysts and xenoliths were carefully removed from all samples using a Frantz isodynamic separator to minimize the presence of extraneous argon. Argon isotope ratios were measured using a VG Isotech© VG3600 mass spectrometer operated in the static mode, connected to extraction and purification lines. Sensitivity of the mass spectrometer was determined by analyzing a known amount of the air standard, which was generally ~1.2×10^7 V/cm^{3}STP. Mass discrimination in the mass spectrometer was corrected assuming ^{40}Ar/^{36}Ar and ^{38}Ar/^{36}Ar of the air standard to be 295.5 and 0.1869, respectively [*Matsumoto and Kobayashi*, 1995]. The initial ^{40}Ar/^{36}Ar is calculated from measured ^{38}Ar/^{36}Ar assuming mass-dependent isotopic fractionation during rock formation. The air standard was analyzed with every sample and a hot blank was measured every five to ten samples. SORI93 biotite was used for calibration of the air standard. Blank levels were less than 1.7×10^{-8} cm^{3}STP for mass 40. No peak drift was observed during analyses. Errors for ^{40}Ar, ^{40}Ar/^{36}Ar and ^{38}Ar/^{36}Ar were estimated from multiple analyses of the air standard, and were 2.0%, 0.2%–0.4% and 0.4%–0.8%, respectively. For measurement of potassium content, a flame emission spectrometer Asahi Rika FP-33D was used in a peak integration mode with a lithium internal standard. Analytical error for potassium measurement is ~2%, estimated from standard deviation of multiple analyses of standard JB-3 and JA-2. See *Ozawa et al.* [2005] for additional information on methods.

A3. University of Massachusetts XRF Analytical Methods

[45] Fifty-two samples were selected for XRF analysis. These samples were unaltered or contained only minor amounts of iddingsite on olivine phenocrysts, and/or calcite, and zeolites in vesicles. For XRF analysis, rocks were broken into small (1–8 mm) fragments in a Rocklabs hydraulic piston crusher between WC plates. Fragments with signs of alteration were removed before powdering the sample. Rock chips were cleaned in a beaker with deionized water and dried in an oven at 70°C for 24 h to drive off excess water. Fragments were powdered in a tungsten carbide mill using a Rocklabs WC shatterbox for 1–3 min.

[46] All XRF analyses were performed at the University of Massachusetts XRF Laboratory where whole-rock, major element abundances were measured using the procedures of *Rhodes and Vollinger* [2004]. One sigma accuracy and precision estimates for the XRF data are ~0.5% for major elements [*Rhodes*, 1996]. Loss on ignition (LOI) analysis represents a measurement of alteration from volatile loss. Five grams of a powdered sample were heated in a muffle furnace at 1020°C for 10 min to limit the amount of ferrous iron formation [*Rhodes and Vollinger*, 2004]. The weight loss is LOI. Major elements were measured on a fused La-bearing lithium borate glass disc using a Siemens MRS-400 spectrometer with a Rh X-ray tube operating at 2700 W. Trace element concentrations (Rb, Sr, Ba, Ce, Nb, Zr, Y, Pb, Zn, Ga, Ni, Cr, V) were measured on a separate powder pellet using a Philips PW2400 sequential spectrometer with a Rh X-ray tube. Precision and accuracy estimates for the trace element data are described by *Rhodes* [1996] and *Rhodes and Vollinger* [2004]. Results for each major element analysis are the average of two separate analyses.

A4. PCIGR Trace Element and Isotopic Analytical Methods

[47] A subset of twenty-four samples was selected for high-precision trace element analysis and Sr, Nd, Pb, and Hf isotopic analysis at the Pacific Centre for Isotopic and Geochemical Research (PCIGR) at the University of British Columbia (UBC; Tables 2 and 3). Samples were selected from the 52 samples analyzed by XRF, based on major and trace element chemistry, alteration (low LOI), and sample location. These samples were powdered in a planetary mill using agate jars and balls that were cleaned with quartz sand between samples.

[48] Samples were prepared for trace element analysis at the PCIGR by the technique described by *Pretorius et al.* [2006] on unleached rock powders. Sample powders (~100 mg) were weighed in 7 mL screw-top Savillex® beakers and dissolved in 1 mL ~14N HNO_3 and 5 mL 48% HF on a hotplate for 48 h at 130°C with periodic ultrasonication. Samples were dried and redissolved in 6 mL 6N HCl on a hotplate for 24 h and then dried and redissolved in 1 mL concentrated HNO_3 for 24 h before final drying. Trace element abundances were measured with a Thermo Finnigan Element2 High Resolution–Inductively Coupled Plasma–Mass Spectrometer (HR-ICP-MS) follow-

ing the procedures described by *Pretorius et al.* [2006] within 24 h of redissolution. High field strength elements (HFSE) and large ion lithophile elements (LILE) were measured in medium resolution mode at 2000x dilution using a PFA Teflon spray chamber washed with Aqua Regia for 3 min between samples. Rare earth elements (REE) were measured in high-resolution mode, and U and Pb in low-resolution mode, at 2000x dilution using a glass spray chamber washed with 2% HNO_3 between samples. Total procedural blanks and reference material (Kil93) was analyzed with the batch of samples. Indium was used as an internal standard in all samples and standard solutions. Background and standard solutions were analyzed after every 5 samples to detect memory effects and mass drift.

[49] Sample digestion for purification of Sr, Nd, Hf, and Pb for column chemistry involved weighing each sample powder. All samples were initially leached with 6N HCl and placed in an ultrasonic bath for 15 min. Samples were rinsed two times with 18 mega Ω cm H_2O between each leaching step (15 total) until the supernatant was clear (following the technique described in detail by *Nobre Silva et al.* [2009]. Samples were then dried on a hotplate for 24 h and weighed again. Sample solutions were then prepared by dissolving ~100–250 mg of the leached powder dissolved in 1 mL ~14N HNO_3 and 10 mL 48% HF on a hotplate for 48 h at 130°C with periodic ultrasonication. Samples were dried and redissolved in 6 mL 6N HCl on a hotplate for 24 h and then dried. Pb was separated using anion exchange columns and the discard was used for Sr, REE, and Hf separation. Nd was separated from the REE and Hf required two additional purification steps. Detailed procedures for column chemistry for separating Sr, Nd, and Pb at the PCIGR are described by *Weis et al.* [2006] and Hf purification is described by *Weis et al.* [2007]. Sr and Nd isotope ratios were measured on a Thermo Finnigan Triton Thermal Ionization Mass Spectrometer (TIMS) in static mode with relay matrix rotation on a single Ta and double Re-Ta filament, respectively. Four to 5 filaments per barrel of 21 were occupied by standards (NIST SRM 987 for Sr and Rennes for Nd) for each barrel where samples were run. Sample Sr and Nd isotopic compositions were corrected for mass fractionation using $^{86}Sr/^{88}Sr = 0.1194$ and $^{146}Nd/^{144}Nd = 0.7219$. Each sample was then normalized using the barrel average of the reference material relative to the values of $^{143}Nd/^{144}Nd = 0.511858$ and $^{87}Sr/^{86}Sr = 0.710248$ [*Weis et al.*, 2006]. During the period when the West Ka'ena samples were analyzed, the Rennes standard gave an average value of 0.511957 ± 26 (n = 18) and NIST SRM 987 standard gave an average of 0.710260 ± 5 (n = 6; 2σ error is reported as times 10^6). $^{147}Sm/^{144}Nd$ ratio errors are approximately ~1.5%, or ~0.006. PCIGR internal reference material from the Pu'u 'Ō'ō eruption of Kīlauea Volcano on 8 July 1993 (Kil93) was processed with the samples and yielded Sr and Nd isotopic ratios of 0.703594 ± 7 and 0.512974 ± 4, respectively. PCIGR internal reference material Ko'olau (base of the Makapu'u section) was also processed with the samples and yielded Sr and Nd isotopic ratios of 0.704086 ± 7 and 0.512760 ± 6, respectively. In both case, the results are within analytical uncertainty of the accepted values (see I. G. Nobre Silva et al., Constraining the origin of the Ninetyeast Ridge, Indian Ocean and its relation with the Kerguelen, Amsterdam and St. Paul hotspots—New insights from new high-precision Pb-Sr-Nd-Hf isotopes, manuscript in preparation, 2010).

[50] Pb and Hf isotopic compositions were analyzed by static multicollection on a Nu Plasma (Nu Instruments) Multiple Collector–Inductively Coupled Plasma–Mass Spectrometer (MC-ICP-MS). The detailed analytical procedure for Pb isotopic analyses on the Nu at the PCIGR is described by *Weis et al.* [2005]. The configuration for Pb analyses allows for collection of Pb, Tl, and Hg together. Tl and Hg are used to monitor instrumental mass discrimination and isobaric overlap, respectively. All sample solutions were analyzed with approximately the same Pb/Tl ratio (~4) as the reference material NIST SRM 981. To accomplish this, a small aliquot of each sample solution from the Pb columns was analyzed on the Element2 to determine the precise amount of Pb available for analysis on the Nu Plasma. The SRM 981 standard was run after every two samples on the Nu Plasma. During the time samples were run, analyses of the SRM 981 Pb reference material gave values of $^{206}Pb/^{204}Pb = 16.9422 \pm 22$, $^{207}Pb/^{204}Pb = 15.4985 \pm 19$, and $^{208}Pb/^{204}Pb = 36.7194 \pm 44$ (n = 38; 2σ error is reported as times 10^4); these values are in excellent agreement with reported TIMS triple-spike values of *Galer and Abouchami* [1998]. Results were further corrected by the sample-standard bracketing method or the ln-ln correction method described by *White et al.* [2000]. Reference material Kil93 yielded Pb isotopic ratios of $^{206}Pb/^{204}Pb = 18.4143 \pm 8$, $^{207}Pb/^{204}Pb = 15.4775 \pm 7$, and $^{208}Pb/^{204}Pb = 38.0697 \pm 18$. Ko'olau reference material yielded Pb isotopic ratios of $^{206}Pb/^{204}Pb =$

17.8375 ± 7, $^{207}Pb/^{204}Pb$ = 15.4339 ± 7, and $^{208}Pb/^{204}Pb$ = 37.7358 ± 16. Both sets of values are in agreement with PCIGR averages [see *Nobre Silva et al.*, 2009, also manuscript in preparation, 2010].

[51] Hf isotopic compositions were analyzed following the procedures detailed by *Weis et al.* [2007]. The configuration for Hf analyses monitored Lu mass 175 and Yb mass 172 to allow for interference correction to masses 174 and 176. Hf isotopic ratios were normalized internally for mass fractionation to a $^{179}Hf/^{177}Hf$ ratio of 0.7325 using an exponential correction. Standards were run after every two samples and sample results were normalized to the ratio of the in-run daily average and a $^{176}Hf/^{177}Hf$ ratio for JMC-475 of 0.282160. During the course of analyses, the Hf standard JMC-475 gave an average value 0.282161 ± 12 (n = 31). Reference materials Kil93 and Ko'olau were processed with the samples and yielded Hf isotopic ratios of 0.283098 ± 5 and 0.282953 ± 5, respectively, and in agreement with PCIGR averages (see Nobre-Silva et al., manuscript in preparation, 2010).

A5. Electron Microprobe Analyses of Olivine

[52] Olivine phenocrysts were measured for the oxides of Si, Fe, Mg, Ca, Ni, and Mn with a JEOL Hyperprobe JXA-8500F at the University of Hawai'i at Mānoa. A minimum of 15 olivine grains were measured in each of 5 selected samples, with 4 analyses on each olivine grain (3 core, 1 rim to check for compositional zoning). The analytical conditions were 20 kV accelerating voltage with long counting times (60 s) for each element and high current of (200 nA) to obtain low detection limits and higher precision (0.01 wt %) following the procedures of *Sobolev et al.* [2007]. San Carlos olivine standard was analyzed as an unknown to monitor accuracy of olivine measurements. Oxide concentrations of all the olivine measurements and the San Carlos olivine standard are presented in the auxiliary material.

Acknowledgments

[53] We would like to thank the science team participants of the Northern Hawaiian Islands Jason2 Expedition in 2007 for contributing to this research. We are also grateful to the Jason2 team from Woods Hole Oceanographic Institute and the crew of the University of Hawai'i research vessel *Kilo Moana*. Insights and advice from James Scoates are greatly appreciated. We are grateful to Brian Jicha and Brad Singer for help with Ar-Ar ages. Thanks to Shichun Huang for providing compiled data for Hawaiian shields, Jane Barling and Bruno Kieffer for assistance with isotope analyses, Claude Maerschalk for sample preparation, Michael Vollinger for XRF analyses, and Eric Hellebrand for help with electron microprobe analyses. We appreciate reviews by Ryoji Tanaka and an anonymous reviewer. This research was supported by a grant from the National Science Foundation to M. Garcia (EAR 05-10482). This paper is SOEST contribution 8040.

References

Abouchami, W., A. W. Hofmann, S. J. G. Galer, F. A. Frey, J. Eisele, and M. Feigenson (2005), Lead isotopes reveal bilateral asymmetry and vertical continuity in the Hawaiian mantle plume, *Nature*, *434*, 851–856, doi:10.1038/nature03402.

Adam, C., V. Vidal, and J. Escartín (2007), 80-Myr history of buoyancy and volcanic fluxes along the trails of the Walvis and St. Helena hotspots (South Atlantic), *Earth Planet. Sci. Lett.*, *261*(3–4), 432–442, doi:10.1016/j.epsl.2007.07.005.

Bianco, T. A., G. Ito, J. M. Becker, and M. O. Garcia (2005), Secondary Hawaiian volcanism formed by flexural arch decompression, *Geochem. Geophys. Geosyst.*, *6*, Q08009, doi:10.1029/2005GC000945.

Blichert-Toft, J., F. A. Frey, and F. Albarède (1999), Hf isotope evidence for pelagic sediments in the source of Hawaiian basalts, *Science*, *285*, 879–882, doi:10.1126/science.285.5429.879.

Blichert-Toft, J., D. Weis, C. Maerschalk, A. Agranier, and F. Albarède (2003), Hawaiian hot spot dynamics as inferred from the Hf and Pb isotope evolution of Mauna Kea volcano, *Geochem. Geophys. Geosyst.*, *4*(2), 8704, doi:10.1029/2002GC000340.

Bryce, J. G., D. J. DePaolo, and J. C. Lassiter (2005), Geochemical structure of the Hawaiian plume: Sr, Nd, and Os isotopes in the 2.8 km HSDP-2 section of Mauna Kea volcano, *Geochem. Geophys. Geosyst.*, *6*, Q09G18, doi:10.1029/2004GC000809.

Clague, D. A., J. G. Moore, J. E. Dixon, and W. B. Friesen (1995), Petrology of submarine lavas from Kilauea's Puna Ridge, Hawaii, *J. Petrol.*, *36*(2), 299–349, doi:10.1093/petrology/36.2.299.

Clague, D. A., J. G. Moore, and J. R. Reynolds (2000), Formation of submarine flat-topped volcanic cones in Hawaii, *Bull. Volcanol.*, *62*, 214–233, doi:10.1007/s004450000088.

Clague, D. A., B. L. Cousens, A. S. Davis, J. E. Dixon, K. Hon, J. G. Moore, and J. R. Reynolds (2003), Submarine rejuvenated-stage lavas offshore Molokai, Oahu, Kauai, and Niihau, Hawaii, *Eos Trans. AGU*, *84*(46), Fall Meet. Suppl., Abstract V11B-01.

Coombs, M. L., D. A. Clague, G. F. Moore, and B. L. Cousens (2004), Growth and collapse of Waianae Volcano, Hawaii, as revealed by exploration of its submarine flanks, *Geochem. Geophys. Geosyst.*, *5*, Q08006, doi:10.1029/2004GC000717.

DePaolo, D. J., and M. Manga (2003), Deep origin of hotspots—The mantle plume model, *Science*, *300*, 920–921.

Eiler, J. M., K. A. Farley, J. W. Valley, A. W. Hofmann, and E. M. Stolper (1996), Oxygen isotope constraints on the sources of Hawaiian volcanism, *Earth Planet. Sci. Lett.*, *144*, 453–468, doi:10.1016/S0012-821X(96)00170-7.

Feigenson, M. D., L. L. Bolge, M. J. Carr, and C. T. Herzberg (2003), REE inverse modeling of HSDP2 basalts: Evidence for multiple sources in the Hawaiian plume, *Geochem. Geophys. Geosyst.*, *4*(2), 8706, doi:10.1029/2001GC000271.

Fitton, J. G., A. D. Saunders, M. J. Norry, B. S. Hardarson, and R. N. Taylor (1997), Thermal and chemical structure of the Iceland plume, *Earth Planet. Sci. Lett.*, *153*, 197–208, doi:10.1016/S0012-821X(97)00170-2.

Frey, F., and J. Rhodes (1993), Intershield geochemical differences among Hawaiian volcanoes: Implications for source compositions, melting process and magma ascent paths, *Philos. Trans. R. Soc. London, Ser. B*, *342*, 121–136.

Frey, F. A., M. O. Garcia, W. S. Wise, A. Kennedy, P. Gurriet, and F. Albarede (1991), The evolution of Mauna Kea volcano, Hawaii: Petrogenesis of tholeiitic and alkalic basalts, *J. Geophys. Res.*, *96*, 14,347–14,375.

Frey, F. A., M. O. Garcia, and M. F. Roden (1994), Geochemical characteristics of Koolau Volcano: Implications of intershield geochemical differences among Hawaiian volcanoes, *Geochim. Cosmochim. Acta*, *58*, 1441–1462, doi:10.1016/0016-7037(94)90548-7.

Gaffney, A. M., B. K. Nelson, and J. Blichert-Toft (2005), Melting in the Hawaiian plume at 1–2 Ma as recorded at Maui Nui: The role of eclogite, peridotite, and source mixing, *Geochem. Geophys. Geosyst.*, *6*, Q10L11, doi:10.1029/2005GC000927.

Galer, S. J. G., and W. Abouchami (1998), Practical application of lead triple spiking for correction of instrumental mass discrimination, *Mineral. Mag.*, *62A*, 491–492, doi:10.1180/minmag.1998.62A.1.260.

Garcia, M. O. (2002), Submarine picritic basalts from Ko'olau Volcano, Hawaii: Implications for parental magma compositions and mantle source, in *Hawaiian Volcanoes: Deep Underwater Perspectives*, *Geophys. Monogr. Ser.*, vol. 128, edited by E. Takahashi et al., pp. 391–401, AGU, Washington, D. C.

Garcia, M. O., J. M. Rhodes, E. W. Wolfe, G. E. Ulrich, and R. A. Ho (1992), Petrology of lavas from episodes 2–47 of the Puu Oo eruption of Kilauea Volcano, Hawaii: Evaluation of magmatic processes, *Bull. Volcanol.*, *55*(1), 1–16.

Garcia, M. O., T. P. Hulsebosch, and J. M. Rhodes (1995), Olivine-rich submarine basalts from the southwest rift zone of Mauna Loa Volcano: Implications for magmatic processes and geochemical evolution, in *Mauna Loa Revealed: Structure, Composition, History, and Hazards*, *Geophys. Monogr. Ser.*, vol. 92, edited by J. M. Rhodes, pp. 219–239, AGU, Washington, D. C.

Garcia, M. O., J. M. Rhodes, F. A. Trusdell, and A. J. Pietruszka (1996), Petrology of lavas from the Puu Oo eruption of Kilauea Volcano: III The Kupaianaha episode (1986–1992), *Bull. Volcanol.*, *58*, 359–379.

Garcia, M. O., A. J. Pietruszka, J. M. Rhodes, and K. Swanson (2000), Magmatic processes during the prolonged Pu'u 'Ō'ō eruption of Kīlauea Volcano, Hawaii, *J. Petrol.*, *41*(7), 967–990.

Garcia, M. O., J. Caplan-Auerbach, E. H. DeCarlo, M. D. Kurz, and N. Becker (2006), Geology, geochemistry, and earthquake history of Lō'ihi Seamount, Hawai'i's youngest volcano, *Chem. Erde*, *66*, 81–108, doi:10.1016/j.chemer.2005.09.002.

Garcia, M. O., et al. (2008), Widespread secondary volcanism around the northern Hawaiian Islands, *Eos Trans. AGU*, *52*, 542–543, doi:10.1029/2008EO520002.

Garcia, M. O., L. Swinnard, D. Weis, A. R. Greene, T. Tagami, H. Sano, and C. E. Gandy (2010), Petrology, geochemistry and geochronology of Kaua'i lavas over 4.5 Myr: Implications for the origin of rejuvenated volcanism and the evolution of the Hawaiian plume, *J. Petrol.*, *51*(7), 1507–1540, http://dx.doi.org/10.1093/petrology/egq027.

Guillou, H., J. Sinton, C. Laj, C. Kissel, and N. Szeremeta (2000), New K-Ar ages of shield lavas from Waianae Volcano, Oahu, Hawaiian Archipelago, *J. Volcanol. Geotherm. Res.*, *96*, 3–4, 229–242, doi:10.1016/S0377-0273(99)00153-5.

Gurenko, A. A., A. V. Sobolev, K. A. Hoernle, F. Hauff, and H.-U. Schmincke (2009), Enriched, HIMU-type peridotite and depleted recycled pyroxenite in the Canary plume: A mixed-up mantle, *Earth Planet. Sci. Lett.*, *277*(3–4), 514–524, doi:10.1016/j.epsl.2008.11.013.

Hanano, D., D. Weis, J. S. Scoates, S. Aciego, and D. J. DePaolo (2010), Horizontal and vertical zoning of heterogeneities in the Hawaiian mantle plume from the geochemistry of consecutive postshield volcano pairs: Kohala-Mahukona and Mauna Kea-Hualalai, *Geochem. Geophys. Geosyst.*, *11*, Q01004, doi:10.1029/2009GC002782.

Hanyu, T., J.-I. Kimura, M. Katakuse, A. T. Calvert, T. W. Sisson, and S. Nakai (2010), Source materials for inception stage Hawaiian magmas: Pb-He isotope variations for early Kilauea, *Geochem. Geophys. Geosyst.*, *11*, Q0AC01, doi:10.1029/2009GC002760.

Haskins, E., and M. Garcia (2004), Scientific drilling reveals geochemical heterogeneity within the Ko'olau shield, Hawai'i, *Contrib. Mineral. Petrol.*, *147*(2), 162–188, doi:10.1007/s00410-003-0546-y.

Hauri, E. H. (1996), Major-element variability in the Hawaiian mantle plume, *Nature*, *382*, 415–419, doi:10.1038/382415a0.

Hearty, P. J., D. B. Karner, P. R. Kenne, S. L. Olson, and S. Fletcher (2005), $^{40}Ar/^{39}Ar$ age of a young rejuvenation basalt flow: Implications for the duration of volcanism and the timing of carbonate platform development during the Quaternary on Kaua'i, Hawaiian Islands, *N. Zeal. J. Geol. Geophys.*, *48*, 199–211.

Herzberg, C. (2005), Mantle geochemistry: Big lessons from little droplets, *Nature*, *436*, 789–790, doi:10.1038/436789b.

Herzberg, C. (2006), Petrology and thermal structure of the Hawaiian plume from Mauna Kea volcano, *Nature*, *444*(7119), 605–609.

Herzberg, C., and P. D. Asimow (2008), Petrology of some oceanic island basalts: PRIMELT2.XLS software for primary magma calculation, *Geochem. Geophys. Geosyst.*, *9*, Q09001, doi:10.1029/2008GC002057.

Hieronymus, C. F., and D. Bercovici (1999), Discrete alternating hotspot islands formed by interaction of magma transport and lithospheric flexure, *Nature*, *397*(6720), 604–607, doi:10.1038/17584.

Hofmann, A. W. (2003), Sampling mantle heterogeneity through oceanic basalts: Isotopes and trace elements, in *The Mantle*, edited by R. W. Carlson, pp. 61–101, Elsevier, Oxford, U. K.

Hofmann, A. W., and K. P. Jochum (1996), Source characteristics derived from very incompatible trace elements in Mauna Loa and Mauna Kea basalts, Hawaii Scientific Drilling Project, *J. Geophys. Res.*, *101*(B5), 11,831–11,839.

Holcomb, R. T., and J. E. Robinson (2004), Maps of Hawaiian Islands exclusive economic zone interpreted from GLORIA Sidescan-Sonar Imagery, scale 1:2,000,000, U.S. Geol. Surv., Washington, D. C.

Huang, S., and F. A. Frey (2005), Recycled oceanic crust in the Hawaiian plume: Evidence from temporal geochemical

variation within the Koolau Shield, *Contrib. Mineral. Petrol.*, *149*, 556–575, doi:10.1007/s00410-005-0664-9.

Huang, S., F. A. Frey, J. Blichert-Toft, R. V. Fodor, G. R. Bauer, and G. Xu (2005), Enriched components in the Hawaiian plume: Evidence from Kahoolawe Volcano, Hawaii, *Geochem. Geophys. Geosyst.*, *6*, Q11006, doi:10.1029/2005GC001012.

Huang, S., W. Abouchami, J. Blichert-Toft, D. A. Clague, B. L. Cousens, F. A. Frey, and M. Humayun (2009), Ancient carbonate sedimentary signature in the Hawaiian plume: Evidence from Mahukona volcano, Hawaii, *Geochem. Geophys. Geosyst.*, *10*, Q08002, doi:10.1029/2009GC002418.

Ito, G. (2001), Reykjanes 'V'-shaped ridges originating from a pulsing and dehydrating mantle plume, *Nature*, *411*, 681–684, doi:10.1038/35079561.

Jackson, M. G., and R. Dasgupta (2008), Compositions of HIMU, EM1, and EM2 from global trends between radiogenic isotopes and major elements in ocean island basalts, *Earth Planet. Sci. Lett.*, *276*(1–2), 175–186, doi:10.1016/j.epsl.2008.09.023.

Kimura, J.-I., T. W. Sisson, N. Nakano, M. L. Coombs, and P. W. Lipman (2006), Isotope geochemistry of early Kilauea magmas from the submarine Hilina bench: The nature of the Hilina mantle component, *J. Volcanol. Geotherm. Res.*, *151*(1–3), 51–72.

Kinzler, R. J., and T. L. Grove (1992), Primary magmas of mid-ocean ridge basalts: 2. Applications, *J. Geophys. Res.*, *97*(B5), 6907–6926.

Kogiso, T., M. M. Hirschmann, and D. J. Frost (2003), High-pressure partial melting of garnet pyroxenite: Possible mafic lithologies in the source of ocean island basalts, *Earth Planet. Sci. Lett.*, *216*(4), 603–617, doi:10.1016/S0012-821X(03)00538-7.

Kogiso, T., M. M. Hirschmann, and M. Pertermann (2004), High-pressure partial melting of mafic lithologies in the mantle, *J. Petrol.*, *45*(12), 2407–2422, doi:10.1093/petrology/egh057.

Koppers, A. A. P. (2002), ArArCALC—Software for $^{40}Ar/^{39}Ar$ age calculations, *Comput. Geosci.*, *28*(5), 605–619, doi:10.1016/S0098-3004(01)00095-4.

Koppers, A. A., and H. Staudigel (2004), Is the Hawaiian-Emperor Bend coeval for all Pacific seamount trails?, *Eos Trans. AGU*, *85*(47), Fall Meet. Suppl., Abstract V51B-0543.

Kuiper, K. F., A. Deino, F. J. Hilgen, W. Krijgsman, P. R. Renne, and J. R. Wijbrans (2008), Synchronizing rock clocks of Earth history, *Science*, *320*, 500–504, doi:10.1126/science.1154339.

Kurz, M. D., J. Curtice, D. E. Lott, and A. Solow (2004), Rapid helium isotopic variability in Mauna Kea shield lavas from the Hawaiian Scientific Drilling Project, *Geochem. Geophys. Geosyst.*, *5*, Q04G14, doi:10.1029/2002GC000439.

Lassiter, J. C., and E. H. Hauri (1998), Osmium-isotope variations in Hawaiian lavas: evidence for recycled oceanic lithosphere in the Hawaiian plume, *Earth Planet. Sci. Lett.*, *164*, 483–496.

Lassiter, J. C., D. J. DePaolo, and M. Tatsumoto (1996), Isotopic evolution of Mauna Kea Volcano: Results from the initial phase of the Hawaii Scientific Drilling Project, *J. Geophys. Res.*, *101*(B5), 11,769–11,780.

Lee, C.-T. A., P. Luffi, T. Plank, H. Dalton, and W. P. Leeman (2009), Constraints on the depths and temperatures of basaltic magma generation on Earth and other terrestrial planets using new thermobarometers for mafic magmas, *Earth Planet. Sci. Lett.*, *279*(1–2), 20–33.

Li, X., R. Kind, Y. Xiaohui, I. Wölbern, and W. Hanka (2004), Rejuvenation of the lithosphere by the Hawaiian plume, *Nature*, *427*, 827–829, doi:10.1038/nature02349.

Longhi, J. (2002), Some phase equilibrium systematics of lherzolite melting: I, *Geochem. Geophys. Geosyst.*, *3*(3), 1020, doi:10.1029/2001GC000204.

Lonsdale, P. (1988), Geography and history of the Louisville hotspot chain in the South Pacific, *J. Geophys. Res.*, *93*(B4), 3078–3104, doi:10.1029/JB093iB04p03078.

MacDonald, G. A., and T. Katsura (1964), Chemical composition of Hawaiian lavas, *J. Petrol.*, *5*, 82–133.

Marske, J. P., A. J. Pietruszka, D. Weis, M. O. Garcia, and J. M. Rhodes (2007), Rapid passage of a small-scale mantle heterogeneity through the melting regions of Kilauea and Mauna Loa volcanoes, *Earth Planet. Sci. Lett.*, *259*, 34–50, doi:10.1016/j.epsl.2007.04.026.

Marske, J. P., M. O. Garcia, A. J. Pietruszka, J. M. Rhodes, and M. D. Norman (2008), Geochemical variations during Kilauea's Pu'u 'O'o eruption reveal a fine-scale mixture of mantle heterogeneities within the Hawaiian plume, *J. Petrol.*, *49*(7), 1297–1318, doi:10.1093/petrology/egn025.

Matsumoto, A., and T. Kobayashi (1995), K-Ar age determination of late Quaternary volcanic rocks using the "mass fractionation correction procedure": Application to the Younger Ontake Volcano, central Japan, *Chem. Geol.*, *125*, 123–135, doi:10.1016/0009-2541(95)00062-Q.

Matsumoto, A., K. Uto, and K. Shibata (1989), K-Ar dating by peak comparison method—New technique applicable to rocks younger than 0.5 Ma, *Bull. Geol. Surv. Jpn.*, *40*, 565–579.

McDonough, W. F., and S. Sun (1995), The composition of the Earth, *Chem. Geol.*, *120*, 223–253, doi:10.1016/0009-2541(94)00140-4.

Montelli, R., G. Nolet, F. A. Dahlen, G. Masters, E. R. Engdahl, and S.-H. Hung (2004), Finite-frequency tomography reveals a variety of plumes in the mantle, *Science*, *303*(5656), 338–343, doi:10.1126/science.1092485.

Moore, J. G., D. Clague, and W. R. Normark (1982), Diverse basalt types from Loihi seamount, Hawaii, *Geology*, *10*, 88–92, doi:10.1130/0091-7613(1982)10<88:DBTFLS>2.0.CO;2.

Moore, J. G., D. A. Clague, R. T. Holcomb, P. W. Lipman, W. R. Normark, and M. E. Torresan (1989), Prodigious submarine landslides on the Hawaiian Ridge, *J. Geophys. Res.*, *94*(B12), 17,465–17,484, doi:10.1029/JB094iB12p17465.

Mukhopadhyay, S., J. C. Lassiter, K. A. Farley, and S. W. Bogue (2003), Geochemistry of Kauai shield-stage lavas: Implications for the chemical evolution of the Hawaiian plume, *Geochem. Geophys. Geosyst.*, *4*(1), 1009, doi:10.1029/2002GC000342.

Nobre Silva, I. G., D. Weis, J. Barling, and J. S. Scoates (2009), Leaching systematics for the determination of high-precision Pb isotope compositions of ocean island basalts, *Geochem. Geophys. Geosyst.*, *10*, Q08012, doi:10.1029/2009GC002537.

Ozawa, A., T. Tagami, and M. O. Garcia (2005), Unspiked K-Ar dating of the Honolulu rejuvenated and Ko'olau shield volcanism on O'ahu, Hawai'i, *Earth Planet. Sci. Lett.*, *232*(1–2), 1–11.

Pearce, J. A. (2008), Geochemical fingerprinting of oceanic basalts with applications to ophiolite classification and the search for Archean oceanic crust, *Lithos*, *100*, 14–48, doi:10.1016/j.lithos.2007.06.016.

Pertermann, M., and M. M. Hirschmann (2003), Anhydrous partial melting experiments on MORB-like eclogite: Phase

relations, phase compositions and mineral-melt partitioning of major elements at 2–3 GPa, *J. Petrol.*, *44*, 2173–2201.

Pietruszka, A. J., and M. O. Garcia (1999), A rapid fluctuation in the mantle source and melting history of Kilauea Volcano inferred from the geochemistry of its historical summit lavas (1790–1982), *J. Petrol.*, *48*(8), 1321–1342.

Pretorius, W., D. Weis, G. Williams, D. Hanano, B. Kieffer, and J. S. Scoates (2006), Complete trace elemental characterization of granitoid (USGSG-2,GSP-2) reference materials by high resolution inductively coupled plasma-mass spectrometry, *Geostand. Geoanal. Res.*, *30*(1), 39–54, doi:10.1111/j.1751-908X.2006.tb00910.x.

Putirka, K. (1999), Melting depths and mantle heterogeneity beneath Hawaii and the East Pacific Rise: Constraints from Na/Ti and rare earth element ratios, *J. Geophys. Res.*, *104* (B2), 2817–2830, doi:10.1029/1998JB900048.

Regelous, M., A. W. Hofmann, W. Abouchami, and S. J. G. Galer (2003), Geochemistry of lavas from the Emperor Seamounts, and the geochemical evolution of Hawaiian magmatism from 85 to 42 Ma, *J. Petrol.*, *44*(1), 113–140.

Reiners, P. W. (2002), Temporal-compositional trends in intraplate basalt eruptions: Implications for mantle heterogeneity and melting processes, *Geochem. Geophys. Geosyst.*, *3*(2), 1011, doi:10.1029/2001GC000250.

Ren, Z., T. Shibata, M. Yoshikawa, K. T. M. Johnson, and E. Takahashi (2006), Isotope compositions of submarine Hana Ridge lavas, Haleakala Volcano, Hawaii: Implications for source compositions, melting process and the structure of the Hawaiian plume, *J. Petrol.*, *47*(2), 255–275, doi:10.1093/petrology/egi074.

Ren, Z., T. Hanyu, T. Miyazaki, Q. Chang, H. Kawabata, T. Takahashi, Y. Hirahara, A. R. L. Nichols, and Y. Tatsumi (2009), Geochemical differences of the Hawaiian shield lavas: Implications for melting process in the heterogeneous Hawaiian plume, *J. Petrol.*, *50*, 1553–1573, doi:10.1093/petrology/egp041.

Rhodes, J. M. (1996), Geochemical stratigraphy of lava flows samples by the Hawaii Scientific Drilling Project, *J. Geophys. Res.*, *101*(B5), 11,729–11,746.

Rhodes, J. M., and S. R. Hart (1995), Episodic trace element and isotopic variations in Mauna Loa lavas: Implications for magma and plume dynamics, in *Mauna Loa Revealed: Structure, Composition, History and Hazards*, *Geophys. Monogr. Ser.*, vol. 92, edited by J. M. Rhodes and J. P. Lockwood, pp. 263–288, AGU, Washington, D. C.

Rhodes, J. M., and M. J. Vollinger (2004), Composition of basaltic lavas sampled by phase-2 of the Hawaii Scientific Drilling Project: Geochemical stratigraphy and magma types, *Geochem. Geophys. Geosyst.*, *5*, Q03G13, doi:10.1029/2002GC000434.

Ribe, N. M., and U. R. Christensen (1999), The dynamical origin of Hawaiian volcanism, *Earth Planet. Sci. Lett.*, *171*(4), 517–531.

Robinson, J. E., and B. W. Eakins (2006), Calculated volumes of individual shield volcanoes at the young end of the Hawaiian Ridge, *J. Volcanol. Geotherm. Res.*, *151*(1–3), 309–317, doi:10.1016/j.jvolgeores.2005.07.033.

Sager, W. W., and B. Keating (1984), Paleomagnetism of Line Islands seamounts: Evidence for Late Cretaceous and Early Tertiary volcanism, *J. Geophys. Res.*, *89*(B13), 11,135–11,151.

Salters, V. J. M., and A. Stracke (2004), Composition of the depleted mantle, *Geochem. Geophys. Geosyst.*, *5*, Q05B07, doi:10.1029/2003GC000597.

Salters, V., J. Blichert-Toft, Z. Fekiacova, A. Sachi-Kocher, and M. Bizimis (2006), Isotope and trace element evidence for depleted lithosphere in the source of enriched Ko'olau basalts, *Contrib. Mineral. Petrol.*, *151*(3), 297–312, doi:10.1007/s00410-005-0059-y.

Sano, H. (2006), Unspiked K-Ar dating of the rejuvenated and shield-building volcanism on Kaua'i, Hawai'i, M.S. thesis, Kyoto Univ., Kyoto, Japan.

Shaw, D. M. (2000), Continuous (dynamic) melting theory revisited, *Can. Mineral.*, *38*(5), 1041–1063, doi:10.2113/gscanmin.38.5.1041.

Sherrod, D. R., J. M. Sinton, S. E. Watkins, and K. M. Brunt (2007), Geologic map of the State of Hawai'i, scale 1:100,000, *U.S. Geol. Surv. Open File Rep., 2007-1089*, 85 pp., 8 plates.

Sleep, N. H. (1992), Hotspot volcanism and mantle plumes, *Annu. Rev. Earth Planet. Sci.*, *20*(1), 19–43, doi:10.1146/annurev.ea.20.050192.000315.

Smith, J. R. (2002), The Kaena Ridge submarine rift zone off Oahu, Hawaii, *Eos Trans. AGU*, *83*(47), Fall Meet. Suppl., Abstract T2062A-1300.

Sobolev, A. V., A. W. Hofmann, and I. K. Nikogosian (2000), Recycled oceanic crust observed in 'ghost plagioclase' within the source of Mauna Loa lavas, *Nature*, *404*, 986–989.

Sobolev, A. V., A. W. Hofmann, S. Sobolev, and I. K. Nikogosian (2005), An olivine-free mantle source of Hawaiian shield basalts, *Nature*, *434*, 590–595.

Sobolev, A. V., et al. (2007), The amount of recycled crust in sources of mantle-derived melts, *Science*, *316*(5823), 412–417, doi:10.1126/science. 1138113.

Staudigel, H. A., A. Zindler, S. R. Hart, T. Leslie, C.-Y. Chen, and D. Clague (1984), The isotope systematics of a juvenile intraplate volcano: Pb, Nd and Sr isotope ratios of basalts from Loihi Seamount, Hawaii, *Earth Planet. Sci. Lett.*, *69*, 13–29, doi:10.1016/0012-821X(84)90071-2.

Steiger, R. H., and E. Jäger (1977), Subcommission on Geochronology: Convention of the use of decay constants in geo- and cosmochronology, *Earth Planet. Sci. Lett.*, *36*, 359–362, doi:10.1016/0012-821X(77)90060-7.

Stille, P., D. M. Unruh, and M. Tatsumoto (1983), Pb, Sr, Nd and Hf isotopic evidence of multiple sources for Oahu, Hawaii basalts, *Nature*, *304*, 25–29, doi:10.1038/304025a0.

Stracke, A., and B. Bourdon (2009), The importance of melt extraction for tracing mantle heterogeneity, *Geochim. Cosmochim. Acta*, *73*(1), 218–238, doi:10.1016/j.gca.2008.10.015.

Tagami, T., Y. Nishimitsu, and D. R. Sherrod (2003), Rejuvenated-stage volcanism after 0.6-m.y. quiescence at West Maui volcano, Hawaii: New evidence from K-Ar ages and chemistry of Lahaina Volcanics, *J. Volcanol. Geotherm. Res.*, *120*, 207–214, doi:10.1016/S0377-0273(02)00385-2.

Tanaka, R., A. Makishima, and E. Nakamura (2008), Hawaiian double volcanic chain triggered by an episodic involvement of recycled material: Constraints from temporal Sr-Nd-Hf-Pb isotopic trend of the Loa-type volcanoes, *Earth Planet. Sci. Lett.*, *265*, 450–465, doi:10.1016/j.epsl.2007.10.035.

Tarduno, J., et al. (2003), The Emperor Seamounts: Southward motion of the Hawaiian hotspot plume in Earth's mantle, *Science*, *301*, 1064–1069, doi:10.1126/science.1086442.

Tatsumoto, M. (1978), Isotopic composition of lead in oceanic basalt and its implication to mantle evolution, *Earth Planet. Sci. Lett.*, *38*, 63–87, doi:10.1016/0012-821X(78)90126-7.

Tilling, R. I., and J. J. Dvorak (1993), Anatomy of a basaltic volcano, *Nature*, *363*, 125–133, doi:10.1038/363125a0.

Van Ark, E., and J. Lin (2004), Time variation in igneous volume flux of the Hawaii-Emperor hot spot seamount chain, *J. Geophys. Res.*, *109*, B11401, doi:10.1029/2003JB002949.

van Keken, P. E., and C. W. Gable (1995), The interaction of a plume with a rheological boundary: A comparison between two-and three-dimensional models, *J. Geophys. Res.*, *100*, 20,291–20,302.

Vervoort, J. D., P. J. Patchett, J. Blichert-Toft, and F. Albarède (1999), Relationships between Lu-Hf and Sm-Nd isotopic systems in the global sedimentary system, *Earth Planet. Sci. Lett.*, *168*, 79–99, doi:10.1016/S0012-821X(99)00047-3.

Vidal, V., and A. Bonneville (2004), Variations of the Hawaiian hot spot activity revealed by variations in the magma production rate, *J. Geophys. Res.*, *109*, B03104, doi:10.1029/2003JB002559.

Walter, M. J. (1998), Melting of garnet peridotite and the origin of komatiite and depleted lithosphere, *J. Petrol.*, *39*(1), 29–60, doi:10.1093/petrology/39.1.29.

Wang, Z., and G. Gaetani (2008), Partitioning of Ni between olivine and siliceous eclogite partial melt: Experimental constraints on the mantle source of Hawaiian basalts, *Contrib. Mineral. Petrol.*, *156*(5), 661–678, doi:10.1007/s00410-008-0308-y.

Watts, A. B., and U. S. ten Brink (1989), Crustal structure, flexure, and subsidence history of the Hawaiian Islands, *J. Geophys. Res.*, *94*, 10,473–10,500.

Weis, D., B. Kieffer, C. Maerschalk, W. Pretorius, and J. Barling (2005), High-precision Pb-Sr-Nd-Hf isotopic characterization of USGS BHVO-1 and BHVO-2 reference materials, *Geochem. Geophys. Geosyst.*, *6*, Q02002, doi:10.1029/2004GC000852.

Weis, D., et al. (2006), High-precision isotopic characterization of USGS reference materials by TIMS and MC-ICP-MS, *Geochem. Geophys. Geosyst.*, *7*, Q08006, doi:10.1029/2006GC001283.

Weis, D., B. Kieffer, D. Hanano, I. N. Silva, J. Barling, W. Pretorius, C. Maerschalk, and N. Mattielli (2007), Hf isotope compositions of U.S. Geological Survey reference materials, *Geochem. Geophys. Geosyst.*, *8*, Q06006, doi:10.1029/2006GC001473.

Wessel, P., and L. W. Kroenke (2007), Reconciling late Neogene Pacific absolute and relative plate motion changes, *Geochem. Geophys. Geosyst.*, *8*, Q08001, doi:10.1029/2007GC001636.

Wessel, P., and L. W. Kroenke (2009), Observations of geometry and ages constrain relative motion of Hawaii and Louisville plumes, *Earth Planet. Sci. Lett.*, *284*(3–4), 467–472, doi:10.1016/j.epsl.2009.05.012.

White, R. (1993), Melt production rates in mantle plumes, *Philos. Trans. R. Soc. London*, *342*(1663), 137–153.

White, W. M., F. Albarède, and P. Télouk (2000), High-precision analysis of Pb isotope ratios by multi-collector ICP-MS, *Chem. Geol.*, *167*, 257–270, doi:10.1016/S0009-2541(99)00182-5.

Wolfe, C. J., S. C. Solomon, G. Laske, J. A. Collins, R. S. Detrick, J. A. Orcutt, D. Bercovici, and E. H. Hauri (2009), Mantle shear-wave velocity structure beneath the Hawaiian hot spot, *Science*, *326*(5958), 1388–1390, doi:10.1126/science.1180165.

Wright, T. L., and F. W. Klein (2006), Deep magma transport at Kilauea volcano, Hawaii, *Lithos*, *87*(1–2), 50–79, doi:10.1016/j.lithos.2005.05.004.

Xu, G., F. A. Frey, D. A. Clague, W. Abouchami, J. Blichert-Toft, B. Cousens, and M. Weisler (2007), Geochemical characteristics of West Molokai shield- and postshield-stage lavas: Constraints on Hawaiian plume models, *Geochem. Geophys. Geosyst.*, *8*, Q08G21, doi:10.1029/2006GC001554.

Yang, H. J., F. A. Frey, and D. A. Clague (2003), Constraints on the source components of lavas forming the Hawaiian North Arch and Honolulu Volcanics, *J. Petrol.*, *44*(4), 603–627, doi:10.1093/petrology/44.4.603.

York, D. (1969), Least-square fitting of a straight line with correlated errors, *Earth Planet. Sci. Lett.*, *5*, 320–324, doi:10.1016/S0012-821X(68)80059-7.

Zou, H., and M. R. Reid (2001), Quantitative modeling of trace element fractionation during incongruent dynamic melting, *Geochim. Cosmochim. Acta*, *65*(1), 153–162, doi:10.1016/S0016-7037(00)00505-6.